Ore Geology Reviews 90 (2017) 970–986

Contents lists available at ScienceDirect

Ore Geology Reviews

journal homepage: www.elsevier.com/locate/oregeo

Genesis of the Jinding Zn-Pb deposit, northwest Yunnan Province, China: Constraints from rare earth elements and noble gas isotopes

Yongyong Tang [a,b], Xianwu Bi [a,*], Mostafa Fayek [b], Finlay M. Stuart [c], Liyan Wu [a], Guohao Jiang [a], Leiluo Xu [a], Feng Liang [a]

[a] State Key Laboratory of Ore Deposit Geochemistry, Institute of Geochemistry, Chinese Academy of Sciences, Guiyang 550081, China
[b] Department of Geological Sciences, University of Manitoba, Winnipeg, MB R3T 2N2, Canada
[c] Scottish Universities Environmental Research Center, East Kilbride G75 0QF, UK

ARTICLE INFO

Article history:
Received 30 May 2016
Accepted 9 April 2017
Available online 27 April 2017

Keywords:
Origin
Noble gas isotopes
Rare earth elements
Jinding
Sanjiang Metallogenic Domain (SMD)

ABSTRACT

The giant sediment-hosted Jinding zinc-lead deposit is located in the Lanping Basin, northwestern Yunnan Province, China. The genesis of the deposit has long been debated and the sources of the ore-forming fluids and metals are controversial. This study presents rare earth element (REE) and noble gas isotope data that constrain the origins of the ore fluids and the heat source driving the hydrothermal circulation. The early-stage sulfides are enriched in light REEs and have high ∑REE values (30.8–94.8 ppm) and weakly negative Eu (δEu 0.85–0.89) and Ce anomalies (δCe 0.84–0.95), suggesting that the fluids were likely derived from dissolution of Upper Triassic marine carbonates with input of REEs from aluminosilicate rocks in the basin. In contrast, the late-stage sulfides have irregular REE patterns, generally low ∑REE values (0.24–10.8 ppm) and positive Eu (δEu 1.22–10.9) and weakly negative Ce anomalies (δCe 0.53–0.90), which suggest that the ore-forming fluids interacted with evaporite minerals. The $^{3}He/^{4}He$ (0.01–0.04 R_a) and $^{40}Ar/^{36}Ar$ values (301–340) of the ore-forming fluids indicate crustal and atmospheric origins for these noble gases. These findings are in agreement with the published fluid inclusion microthermometry data and the results of H, O, C, S, Pb and Sr isotope studies. Our data, in combination with published results, support a two-stage hydrothermal mineralization model, involving early-stage basinal brines and late-stage meteoric water that acquired metals and heat from crustal sources.

1. Introduction

The Sanjiang Metallogenic Domain (SMD) in southwestern China underwent multiple stages of openings and closures of the Tethys oceans from late Paleozoic to Mesozoic and the India-Asia continental collision in Cenozoic, resulting in a characteristic landscape of basins in high mountain terrains and parallel drainage of three rivers (i.e., Nujiang, Lancangjiang and Jinshajiang), together with the formation of economically significant metal deposits (Deng et al., 2014, 2016; Hou et al., 2007; Wang et al., 2016). Sediment-hosted base metal deposits mainly occur in Mesozoic-Cenozoic sedimentary basins within SMD, including the world-class Jinding deposit (Zn-Pb-Sr-Ag-Cd-Tl) and others such as, Baiyangping (Cu-Ag-Pb-Zn-Co), Jinman (Cu-Ag-Mo), Lanuoma (Pb-Zn-Sb), Zhaofayong (Pb-Zn), Mohailaheng (Pb-Zn). Many researches consider these mineral systems to differ from the typical Mississippi Valley-type lead-zinc deposits (MVT), sedimentary exhalative lead-zinc deposits (SEDEX), sandstone lead deposits (SST) and sediment-hosted stratiform copper deposits (SSC) in terms of geological setting, ore-controlling style, host rock and metal sources (He et al., 2009; Hou et al., 2008; Song et al., 2011; Tao et al., 2011; Wang et al., 2009a; Xue et al., 2007). These mineral systems generally formed during the Cenozoic India-Asia continental collision (e.g., Liu et al., 2016; Tian et al., 2009; Wang et al., 2011; Zhang et al., 2013; Zou et al., 2015) and have experienced little modification since their formation (Hou et al., 2008; Song et al., 2011). Therefore, they provide a good case studying and understand the genesis of large sediment-hosted base metal mineralization processes. The proposed formation styles for these sediment-hosted deposits range from syndepositional to post-depositional stratabound (e.g., Bai et al., 1985), mixing of crust- and mantle-derived fluids (e.g., Wang and Li, 1991; Xue et al., 2003; Yin et al., 1990), MVT-like (e.g., Liu et al., 2013; Song et al., 2011), orogenic type (e.g., Hou et al., 2008) and polymetallic vein type (Cu deposit, e.g., Song et al., 2011).

Jinding is the largest Zn-Pb deposit in China, and probably the youngest giant sediment-hosted Zn-Pb deposit in the world (Xue

* Corresponding author.
E-mail address: bixianwu@vip.gyig.ac.cn (X. Bi).

http://dx.doi.org/10.1016/j.oregeorev.2017.04.024
0169-1368/

et al., 2007). It contains 16 Mt of Zn-Pb resources, with an average grade of 7.3%, and significant amounts of Tl (8167 t), Cd (170,000 t), Ag (1722 t) and Sr (1.47 Mt) (The Yunnan Jinding Zn Ltd Corporation, 2008; Xue et al., 2002). Most recently, Leach et al. (2016) proposed that the Jinding deposit is a sub-type of MVT deposits developed in an evaporite diapiric environment. In the past few decades, numerous studies have focused on the genesis of this deposit. However, some fundamental questions remain, including the origin of the mineralizing fluids and the sources of the metals and heat. Previous isotopic studies, including on sulfur (Wu and Wu, 1989; Yang, 2013; Zhao, 1989), lead (Qin and Zhu, 1991; Zhang, 1993; Zhao, 1990; Zhou and Zhou, 1992) and noble gas isotopes (Wang et al., 2004; Xue et al., 2003), have proposed that mantle-derived fluids and metals participated in the hydrothermal processes leading to the mineralization. However, recent studies using state-of-the-art analytical techniques have questioned this hypothesis. For example, *in situ* S isotopic measurements of sulfides show varying and negative $\delta^{34}S$ values, which can only be generated by bacterial sulfate reduction and thermochemical sulfate reduction, with no evidence of magmatic sulfur (Tang et al., 2014). High-precision lead isotope data display a limited range, consistent with a purely crustal origin (Tang et al., 2013b; Wang et al., 2009a; Xiu et al., 2006; Zhao, 2006).

Helium isotopes are perhaps the most sensitive tracer of mantle volatiles (and heat) in crustal fluids (Hu et al., 1998; Turner and Stuart, 1992; Stuart et al., 1994, 1995). However, the He isotopic data of Xue et al. (2003) and Wang et al. (2004) differ markedly from those by Hu et al. (1998), leading to contrasting views of the role of mantle-derived components and, consequently, the thermal source associated with the circulating ore fluids. These controversies have complicated our understanding of the mineralization processes and the development of a model.

In this paper, we present the rare earth element (REE) compositions of sulfides from different mineralization stages and the noble gas isotopic compositions of the mineralizing fluids hosted in late-stage galena. These data place new constrains on the source of the ore-forming materials and heat in the Jinding deposit.

2. Background

2.1. Regional geology

The SMD is located at the east end of the Himalaya-Tethys tectonic domain and at the conjunction between the Tethyan Mountain Chain and the Circum-Pacific Mountain Chain (Mo et al., 1994). The region is connected to the South China Block to the east, the Indochina and Sibumasu Blocks to the south, the Lhasa Block to the west, and the Songpan-Ganzê fold belt and East and West Qiangtang Blocks to the north (Fig. 1). The Lanping-Simao Basin, bounded by the Jinshajiang-Ailaoshan fault to the east and the Lancangjiang fault to the west, is a NNW-trending intracontinental basin that developed on the Changdu-Lanping-Simao microplate. The basin is cut by the Lanping-Simao fault (the Axis Fault), which is thought to penetrate from the shallow crust to the mantle (Yin et al., 1990).

The Lanping Basin experienced three stages of tectonic evolution: basement formation, intracontinental basin development, and transition of basin and orogen (Fu, 2005; Mou et al., 1999; Tao et al., 2002; Zhang et al., 2010). The basement rocks are rarely exposed because of thick Mesozoic-Cenozoic cover, but they are generally presumed to be composed of Proterozoic metamorphic rocks, similar to the basement of the Yangtze Plate (Mu et al., 1999). The basin is filled with more than 10 km of Mesozoic-Cenozoic sediments: Upper Triassic marine clastics, carbonates, and sandy mudstones; Jurassic marine-terrestrial red clastics and minor carbonates; Cretaceous shallow lacustrine red clastics; and Cenozoic siliciclastic rocks (Liao and Chen, 2005; Mu et al., 1999). Several evaporite horizons are present in the Middle-Upper Triassic, Middle-Upper Jurassic and Paleocene sequences (Gao, 1991; Xue et al., 2007). The India-Asia collision in the Cenozoic folded and thrusted the Mesozoic rocks into nappes that overlie Neogene sequences.

Paleozoic arc-related volcanic-sedimentary sequences are exposed along the margins of the Lanping-Simao Basin. They record the subduction of oceanic crust on both sides in the late Permian (Mo et al., 1994). Continent-arc collision in the Early Triassic was followed by post-collisonal extension in the Middle to Late Triassic, which resulted in bimodal arc volcanism (Pan et al., 2003). Cenozoic dominantly alkaline rocks, consisting of quartz syenite, rhyolite, granite porphyry and trachyte (68–23 Ma, Xue et al., 2003), are present mainly along the eastern margin of the Lanping Basin. A few exposures of contemporaneous magmatism within the basin have been reported (e.g., Zhuopan, Zaojiaochang, Lv and Qian, 1999; Teng et al., 2001; Zhang et al., 2000). No igneous rocks crop out in or near the Jinding deposit.

2.2. Deposit geology

The Jinding deposit developed within a secondary doming structure west of the Pijiang fault, a northern section of the Lanping-Simao fault (Figs. 1 and 2). A thrust fault (F_2) separates the Mesozoic-Cenozoic rocks of the mineralized region into a lower autochthonous normal sequence and an upper allochthonous overturned sequence. The allochthon is composed of Upper Triassic, Middle Jurassic and Lower Cretaceous sedimentary units. The Upper Triassic rocks include three sections: (i) the upper section, composed of mudstones, siltstones and sandstones (*Maichuqing Fm.*); (ii) the middle section, composed of marls, limestones, and bituminous limestones with tuffaceous sandstones (*Sanhedong Fm.*); and (iii) the lower section, composed of sandstones, siltstones, mudstones, and interlayered conglomerates (*Waigucun Fm.*). The Middle Jurassic is dominantly composed of mudstones, siltstones, and sandstones of the Huakaizuo Fm., which underlies the Triassic rocks. The Lower Cretaceous Jingxing Fm. comprises sandstones. A series of thrust faults parallel to F_2 dislocated the lithologies within the nappes. The autochthon consists of the Paleocene Yunlong Fm. and the Upper Cretaceous Hutousi and Nanxin formations. The Yunlong Fm. consists of limestone breccias and limestone fragment-bearing sandstones to the east of the mineralized area and sandstones and evaporitic mudstones to the west. The Hutousi Fm. comprises fine-grained quartz sandstone and is unconformably overlain by the Yunlong Fm. The underlying Nanxin Fm. is composed of rhythmically interbedded conglomerates, sandstones and siltstones.

Over a hundred orebodies are present in Beichang, Paomaping, Jiayashan, Fengzishan, Xipo, Nanchang and Baicaoping around the dome structure. The Beichang block accounts for approximately 75% of the total ore reserves (Third Geological Team, 1984). The mineralization is structurally controlled by F_2 and occurs in both the hanging wall and footwall. The hanging wall mineralization largely occurs in the Lower Cretaceous Jingxing Fm. and is referred to as the upper ore zone, which is generally strata-bound or tabular in shape. The footwall orebodies are typically lenses and veins that are mainly hosted in the upper section of the Yunlong Fm., also known as the lower ore zone. Celestine and anhydrite-gypsum ores are developed around the Zn-Pb mineralization or in nearby host rocks (Fig. 2b).

The sulfide mineralization is largely disseminated and massive vein types (Figs. 3 and 4), with the disseminated type accounting for the majority of the ore occurrences, especially in the upper ore zone. The disseminated ore consists of fine-grained sulfides (spha-

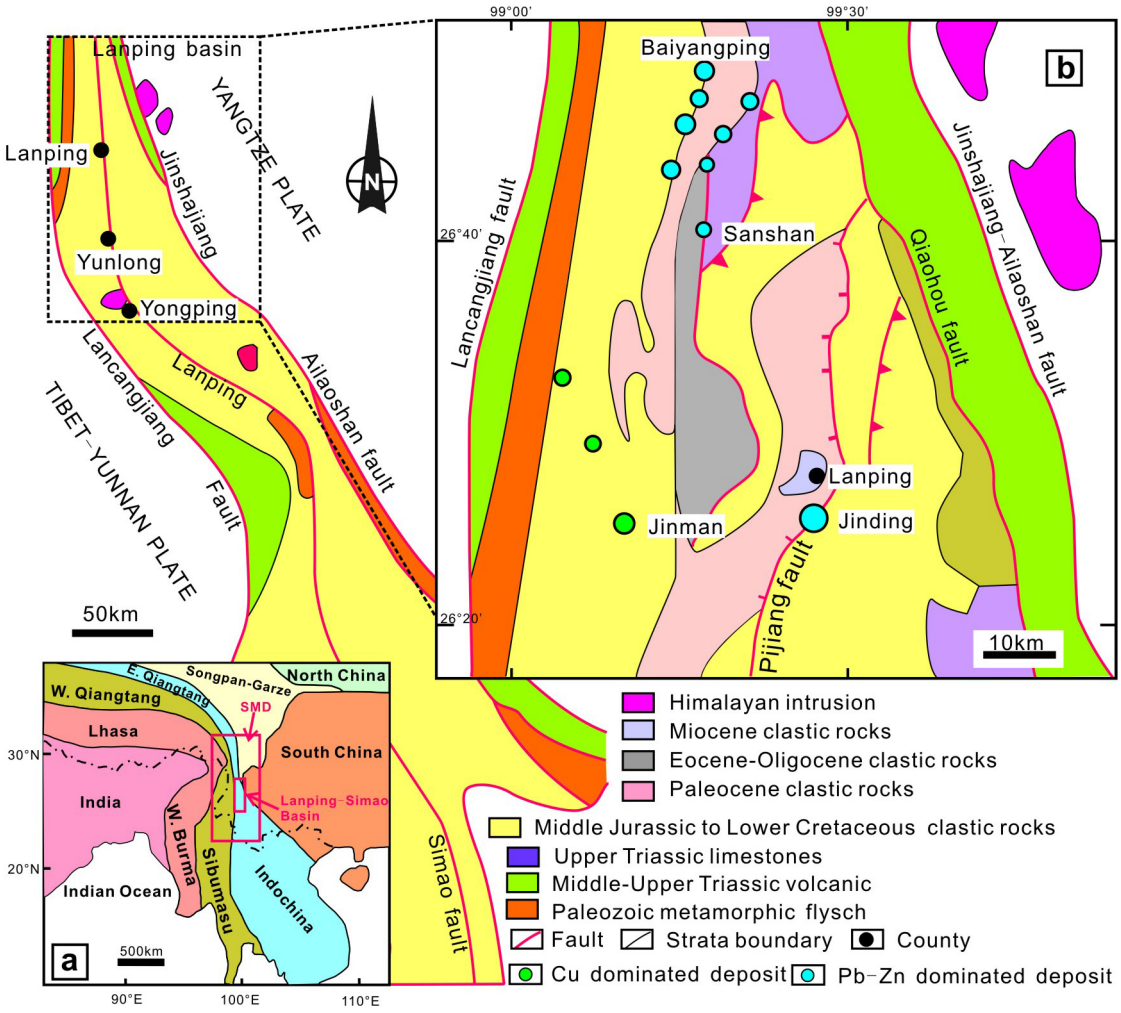

Fig. 1. Tectonic framework of the Sanjiang Metallogenic Domain (SMD) showing the position of the Lanping-Simao Basin (a), and the geological map of the Lanping-Simao Basin with an enlargement of the northern Lanping basin (b), which shows the distributions of the stratigraphic units, faults and the major Pb-Zn and Cu deposits (modified after Hou et al., 2007; Xue et al., 2007).

lerite, galena and pyrite) in sandstones (Fig. 3a). The sulfides occur as secondary cements in sandstone matrix, commonly replacing diagenetic calcareous cement (Fig. 4a-b) and occasionally K-feldspar (Fig. 4c), albite and quartz. The most common sulfides in the sandstones are sphalerite and pyrite, followed by galena. In some high-grade sandstone ores, the matrix is fully replaced by sulfides.

The massive vein ores are restricted to the eastern part of the deposit and occur along dissolution voids, fractures and cavities in sandstones and carbonate breccias. The ore occurs mainly within the lower ore zone. The breccias include blocks of bituminous limestone, dolomitic limestone, siliceous dolomite, siltstone and mudstone that are poorly-sorted, subangular to angular in shape, 1–100s of *cm* in size and rarely mineralized (Fig. 3b). The spaces between the brecciated blocks are filled with fine-grained sandstone ore or massive-vein sulfides, which are not evenly mineralized but often have high grades. Sphalerite commonly occurs as coarse crystals intergrown with pyrite and galena, in association with euhedral calcite. Coarse-grained galena veins commonly cut disseminated sphalerite in sandstones (Fig. 3c) or massive sphalerite in limestone breccias (Fig. 3d and Fig. 4d), indicating the sphalerite crystallized earlier than the galena. Coarse-grained vuggy celestine, occasionally replaced by calcite, is coeval with galena, which is associated with bitumen in voids and fractures (Fig. 3e-f). Less frequently, veinlets of barite appear to be coeval with galena that crosscut massive sphalerite (Fig. 4f).

The Jinding deposit is believed to have formed through complex processes, including early diagenesis followed by hydrothermal mineralization and supergene oxidization (e.g., Luo et al., 1994; Zhao, 2006). Based on a study of ore textures and cross-cutting and paragenetic relationships of the primary minerals, the hydrothermal process has been divided into early and late stages (Fig. 5). The early stage occurs as fine-grained (30–70 *um*) sphalerite, pyrite and galena, accompanied by largely silicification in sandstones, or occurs as massive sphalerite intergrown with pyrite, galena and calcite in sandstones and carbonate breccias. The predominant mineral is sphalerite, followed by pyrite and galena. In sharp contrast, the late stage mineralization is characterized by coarse-grained lead-dominated massive- or vein-type mineralization and the abundant presence of sulfate minerals. Late-stage galena occurs as veins that crosscut the early-stage mineralization, or as isolated euhedral grains within calcite and celestine vugs. These galena grains are usually >100 *um*. Late-stage sphalerite is less abundant relative to galena, and is coarsely crystalline in association with hydrothermal calcite, celestine and bitumen.

3. Analytical methods

The ore samples were collected from underground mine workings. Mineral separates were obtained by conventional separation techniques and by subsequent handpicking under a binocular

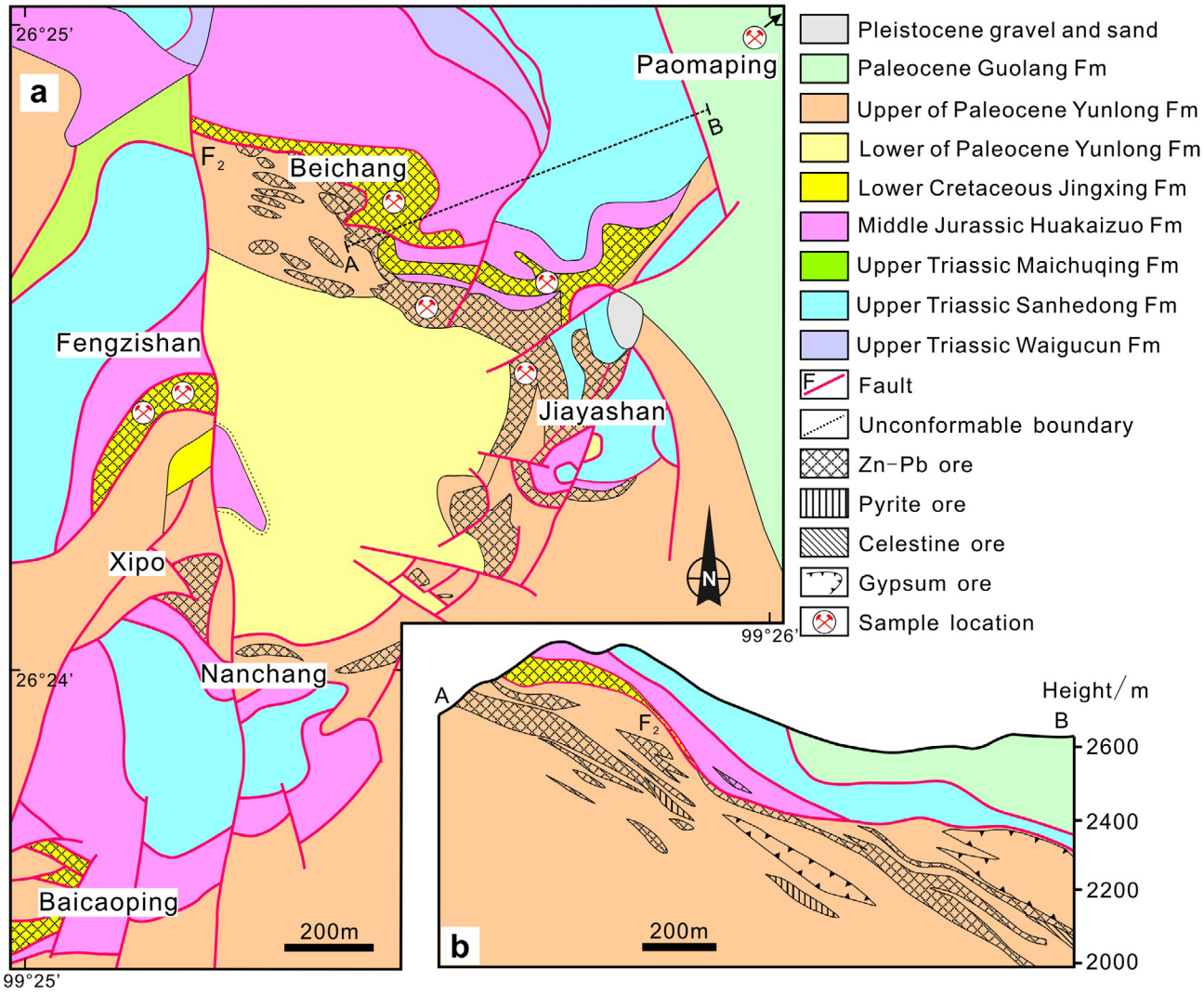

Fig. 2. Geological map of the Jinding Zn-Pb deposit (a) and a typical cross-section of A-B (b) showing the spatial relationship between sulfide and sulfate ores (modified after Third Geological Team, 1984).

microscope. Sample purity was checked using powder X-ray diffraction. Early-stage fine-grained disseminated sphalerite and late-stage sphalerite and galena were chosen for REE analysis. In addition, the REE compositions of the host-rocks in the mining area were also analyzed. Noble gas isotopic analysis was performed on the late stage coarse galena.

3.1. Rare earth element analysis

The REEs in sulfide samples were analyzed at the Analysis and Testing Center, Beijing Research Institute of Uranium Geology (CNNC, China National Nuclear Corporation) using a high-resolution inductively coupled plasma mass spectrometer (ICP-MS; Finnigan MAT Co., Germany). Approximately 50 mg of sample was dissolved with 1 ml HF and 1 ml HNO_3 at 190 °C for 36 h. After evaporation, the sample was redissolved in 1 ml HNO_3 and then dried. After 500 ng of Rh was added as an internal standard solution, 2 ml HNO_3 and 3 ml deionized water were added and heated at 140 °C for 5 hours. Then, 0.4 ml of this solution was centrifuged and brought to 10 ml with deionized water for ICP-MS measurements (Qi and Conrad, 2000). The host-rock samples were analyzed at the Institute of Geochemistry, Chinese Academy of Sciences (IGCAS) following a similar procedure. The results generally have uncertainties of less than 5%.

3.2. Noble gas isotopes

The noble gas isotope compositions of fluid inclusions in galena were measured at the IGCAS and the Scottish Universities Environmental Research Center (SUERC), UK. At the IGCAS 0.5–1 g of 1–2 mm galena grains were baked at ~150 °C under ultra-high vacuum for more than 24 h prior to analysis. The samples were then crushed in an apparatus manufactured from modified Nupro-type valves (Stuart et al., 1995). The gases were released into the all-metal extraction system, where they were exposed first to a titanium sponge furnace at 800 °C for 20 min to remove the bulk of active gases (e.g., H_2O and CO_2), and then to two SAES Zr-Al getters (one at room temperature and the other at 450 °C) for 10 min for further purification. An activated charcoal cold finger was used to separate He from Ar at the temperature of liquid N_2 (−196 °C) for 40–60 min to trap Ar. He and Ar isotopes were measured using a VG5400 mass spectrometer. The He and Ar abundances and isotopic ratios were calibrated against aliquots of 0.1 cm^3 STP air (5.2×10^{-7} cm^3 STP ^4He and 9.3×10^{-4} cm^3 STP ^{40}Ar). The procedural blank was less than 2×10^{-10} cm^3 STP ^4He

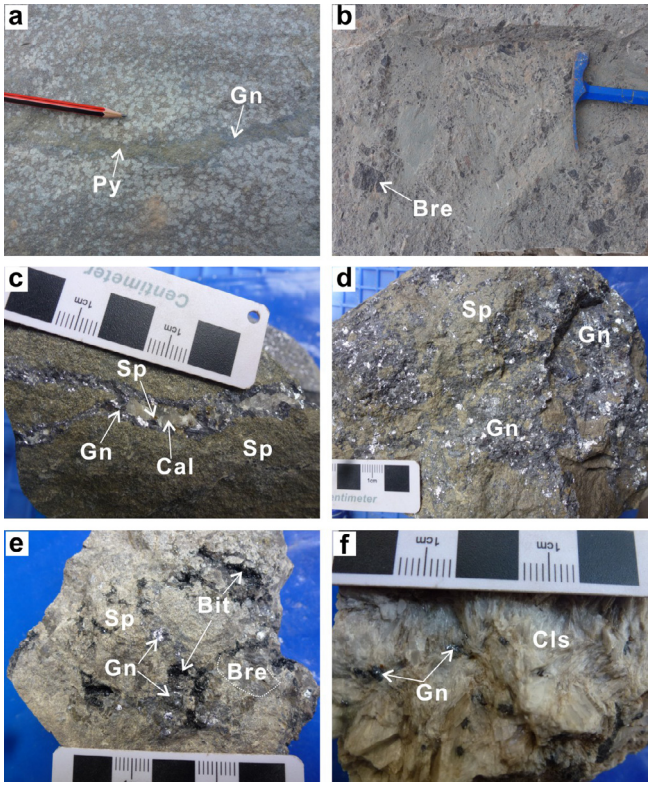

Fig. 3. Hand specimens of major ore occurrences from the Jinding deposit. a. Disseminated ore in sandstone, cut by a late galena and pyrite vein. White spots are quartz, and sulfides occur as cement interstitial to quartz. b. Breccia-bearing sandstone ore, in which the breccia clasts are composed of bituminous limestone, free of mineralization, and cemented by fine-grained sandstone containing early-stage disseminated sulfides. c. Early-stage disseminated sandstone ore is crosscut by a late-stage coarse-grained galena vein, accompanied by calcite and sphalerite. d. Massive ore where late-stage galena infill fractures and replaces early-stage sphalerite. e. Limestone breccia cemented by sphalerite, and dissolution cavities and fractures filled with late-stage coarse-grained galena associated with bitumen. f. Massive celestine ore intercalated with late-stage euhedral galena. Abbreviations: Bit-Bitumen, Cal-calcite, Cls-celestine, Gn-galena, Bre-breccia, Py-pyrite, Sp-sphalerite.

and $(2–4) \times 10^{-10}$ cm^3 STP ^{40}Ar, and constituted less than 1% of the volume of the analyses, which is too low to affect the calibration of the abundance measurements.

The gas extraction and analysis procedure at SUERC was similar to that of IGCAS. Helium isotopes were analyzed using a high-resolution dual collector Thermo HELIX-SFT mass spectrometer that is specifically designed for measuring low ^{3}He concentrations in the presence of a high ^{4}He beam size. Isotope ratios were calibrated against pipettes taken from a reservoir of the HESJ standard. Blank levels never exceeded 1×10^{-11} cm^3 STP ^{4}He and were trivial in comparison to the measured amounts.

4. Results

4.1. REEs

Early-stage sphalerite is enriched in light REEs (LREE) and have higher total REE (∑REE) values (30.8–94.8 ppm, mean 55.3 ppm, n = 4), constant LREE/heavy REE (HREE) ratios (7.97–9.54, mean 8.48), weakly negative Eu anomalies (δEu 0.85–0.89, mean 0.87), and weakly negative Ce anomalies (δCe 0.84–0.95, mean 0.89). The REE patterns of the late-stage sulfides are irregular (Fig. 6). They have lower ∑REE values (0.24–10.8 ppm, mean 3.0 ppm, n = 8), a wide range of LREE/HREE ratios (1.85–14.5, mean 8.72), positive Eu anomalies (δEu 1.22–10.9, mean 4.17) and negative Ce anomalies (δCe 0.53–0.90, mean 0.71). In contrast, the host rocks, except for the carbonates, show relatively high REE contents. The siliciclastic sedimentary rocks of the Jurassic, Cretaceous and Paleogene have similar REE patterns, which display LREE-enriched patterns with ∑REE values ranging from 71 to 187 ppm (mean 143 ppm, n = 6), moderately negative Eu anomalies (δEu 0.62–0.75, mean 0.69) and no or weakly positive Ce anomalies (δCe 0.95–1.04, mean 1.01). The carbonate rocks are depleted in REEs (∑REE 17.3–35.6 ppm, mean 23.2, n = 4) relative to the siliciclastic sedimentary rocks. In addition, they are also characterized by weakly negative Ce anomalies (δCe 0.76–0.89, mean 0.77). The results are shown in Table 1.

4.2. Noble gas isotopes

The results of He isotope compositions of the fluid inclusions in the late-stage galena obtained from the two independent laboratories are in good agreement (Table 2). The ^{4}He concentrations are $(0.24–18.3) \times 10^{-7}$ cm^3 STPg^{-1}, and the ^{3}He/^{4}He ratios range from 0.01 to 0.04 R_a. The concentrations of ^{40}Ar are $(1.65–10.0) \times 10^{-7}$ cm^3 STPg^{-1}, and the ^{40}Ar/^{36}Ar ratios vary from 301 to 340. Our data are consistent with the data from pyrite obtained by Hu et al. (1998), who found ^{3}He/^{4}He ratios between 0.03 R_a and 0.06 R_a, and ^{40}Ar/^{36}Ar ratios between 301 and 653. These data are within the range of crustal He values (Fig. 7). However, the data differ are from those reported in Xue et al. (2003) and Wang et al. (2004), who reported values that are significantly different from crustal noble gas values.

5. Discussion

5.1. Source of ore-forming materials

5.1.1. Constraint from REE

The REE compositions of sulfide minerals are generally controlled by the composition of the parental fluid and the physicochemical conditions (e.g., T, P, pH, and Eh) of the depositional environment of the sulfide minerals (Bau and Dulski, 1999; Douville et al., 1999; Mills and Elderfield, 1995). The samples from the early-stage mineralization of the Jinding deposit have relatively high REE contents, LREE enrichments, and weakly negative Eu and Ce anomalies, whereas those from the late-stage mineralization show lower and more variable REE contents, positive Eu anomalies and negative Ce anomalies (Fig. 6a-b). The negative Ce anomalies were interpreted to be derived from mantle sources (Wang and Li, 1991). However, this contrasts with the H, O, C, S, Pb and Sr isotopic results, as well as the noble gas isotope data. A negative Ce anomaly requires the decoupling of Ce from its REE neighbors following the transformation of Ce (III) to Ce (IV) compounds, which behave differently from REE (III) compounds during mobilization, transport and fixation. One possibility is that negative Ce anomalies may have been produced during the deposition of sulfides from a solution in which Ce was oxidized and removed. However, early-stage sulfides were likely precipitated in a low-f_{O2} environment based on mineral paragenesis (Fig. 5) and the fluid inclusion data suggest that early-stage fluids were reducing, with Eh values ranging from −0.49 to −0.40 V (Wen et al., 1995). Therefore, the negative Ce anomalies are less likely to be a result of Ce (III) oxidation in the fluids. The alternative explanation is that the values were inherited from the fluid from which the sulfides precipitated. The fluid may have acquired negative Ce anomalies either during REE mobilization from a source rock, e.g., Ce was fixed as a relatively insoluble Ce (IV) compound, or the fluid removed REEs from a source rock that was itself

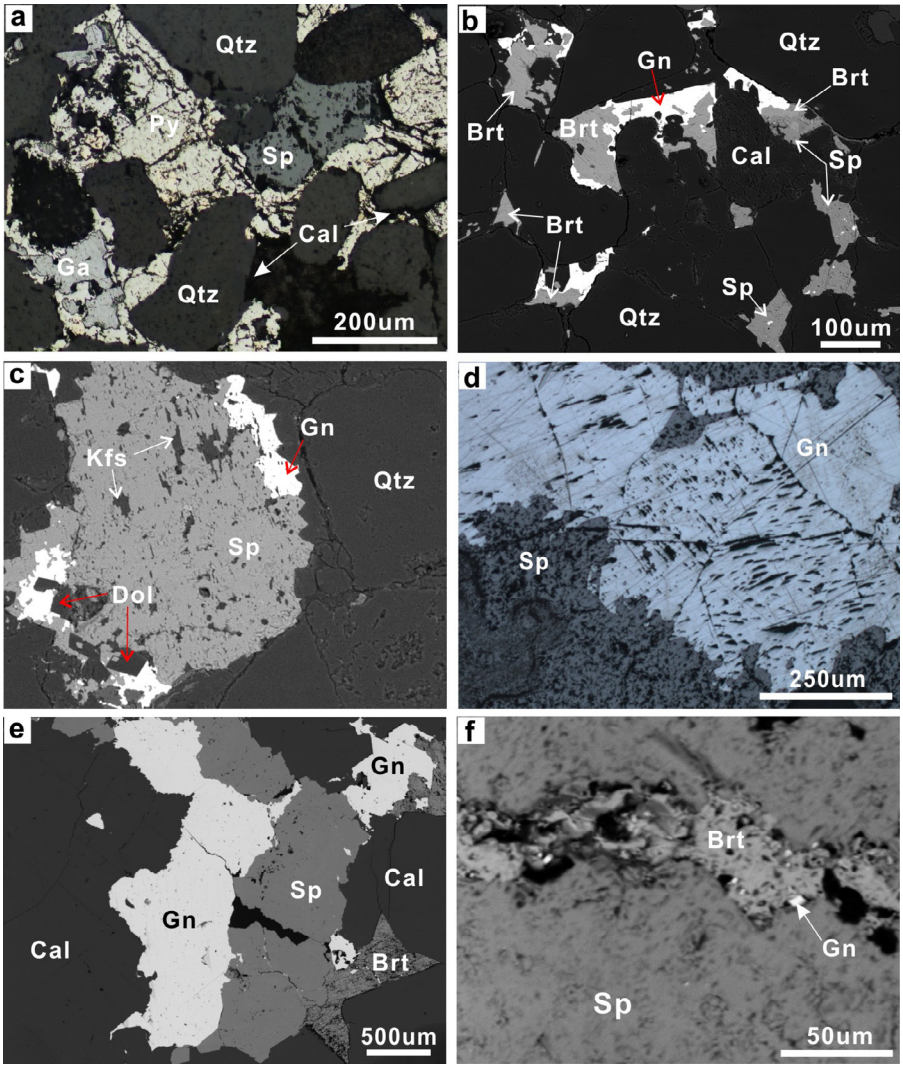

Fig. 4. a. Early-stage disseminated sulfides replacing original calcite cement between quartz clasts in sandstone (reflected light). b. Early-stage sandstone-hosted disseminated sulfides occurring interstitial to quartz, where barite is replaced by galena and sphalerite (back-scattered image). c. Potash feldspar is replaced by sphalerite and galena with metasomatic relics texture in sandstones (back-scattered image). d. Late-stage galena cutting early-stage massive sphalerite (reflected light). e. Late-stage galena and sphalerite, associated with barite in limestone breccia (back-scattered image). f. Late-stage barite veinlet intergrown with galena crosscutting early-stage massive sphalerite (back-scattered image). Abbreviation: Brt-barite, Dol-dolomite, Kfs-potash feldspar, Qtz-quartz.

already depleted in Ce, or the fluid may have preferentially lost Ce during fluid-wall rock interaction (Bau et al., 2003). The negative Ce anomalies in the fluid likely did not result from igneous rocks or clastic sediments because Ce (III) is generally dominant in such lithologies and the amount of Ce (IV) is extremely low. Scavenging by oxidation is also unlikely to lead to preferential Ce loss during fluid migration because Ce (III) compounds are more stable than Ce (IV) hydroxide complexes at elevated temperatures (Bilal and Müller, 1992). Marine carbonate rocks are the most likely source of the REEs because the negative Ce anomalies in carbonates, inherited from the seawater from which they precipitated (Bau et al., 2003), could have been passed down to the descendant fluids.

The REE patterns of the early-stage sulfides remain consistent with those of the associated calcite (Tang et al., 2011), which also argue that the negative Ce anomalies were probably linked to a carbonate-rich alkaline fluid produced from dissolution of marine carbonates. Although the REE patterns of both sulfides and calcites are similar to those of carbonate rocks around the Jinding deposit (Fig. 6c), the relatively low concentrations of REEs in the carbonates were probably not enough to produce the high concentrations of REEs in the sulfides. Therefore, some other source, such as aluminosilicates, likely contributed REEs to the fluids because these lithologies generally have REE values several orders of magnitude higher than that of marine carbonates. In the Lanping-Simao Basin, REEs are found generally enriched in the sandstones and siltstones (average 168 ppm, Li et al., 1995), and some local mafic igneous rocks are also reported as a potential source because their REE contents can be as high as over 1000 ppm (Teng et al., 2001).

In contrast, the late-stage sulfide samples are characterized by positive Eu anomalies and low REE contents. Positive Eu anomalies typically occur in hydrothermal solutions at temperatures above 200–250 °C due to the formation of a significant amount of Eu (II) after decoupling from its REE neighbors (Bau and Moller, 1992). Allowing for the fluid inclusion homogenization temperatures that are <200 °C for the late-stage mineralization (Fig. 8), the presence of positive Eu anomalies suggests that the fluids experienced higher temperatures prior to formation or arose from interactions with positive Eu anomaly-bearing minerals. Similar features are also reported in the Jinman and Fulongchang deposits, where the positive Eu anomalies are considered to have resulted from the interaction of ore fluids with basinal sedimentary sulfates

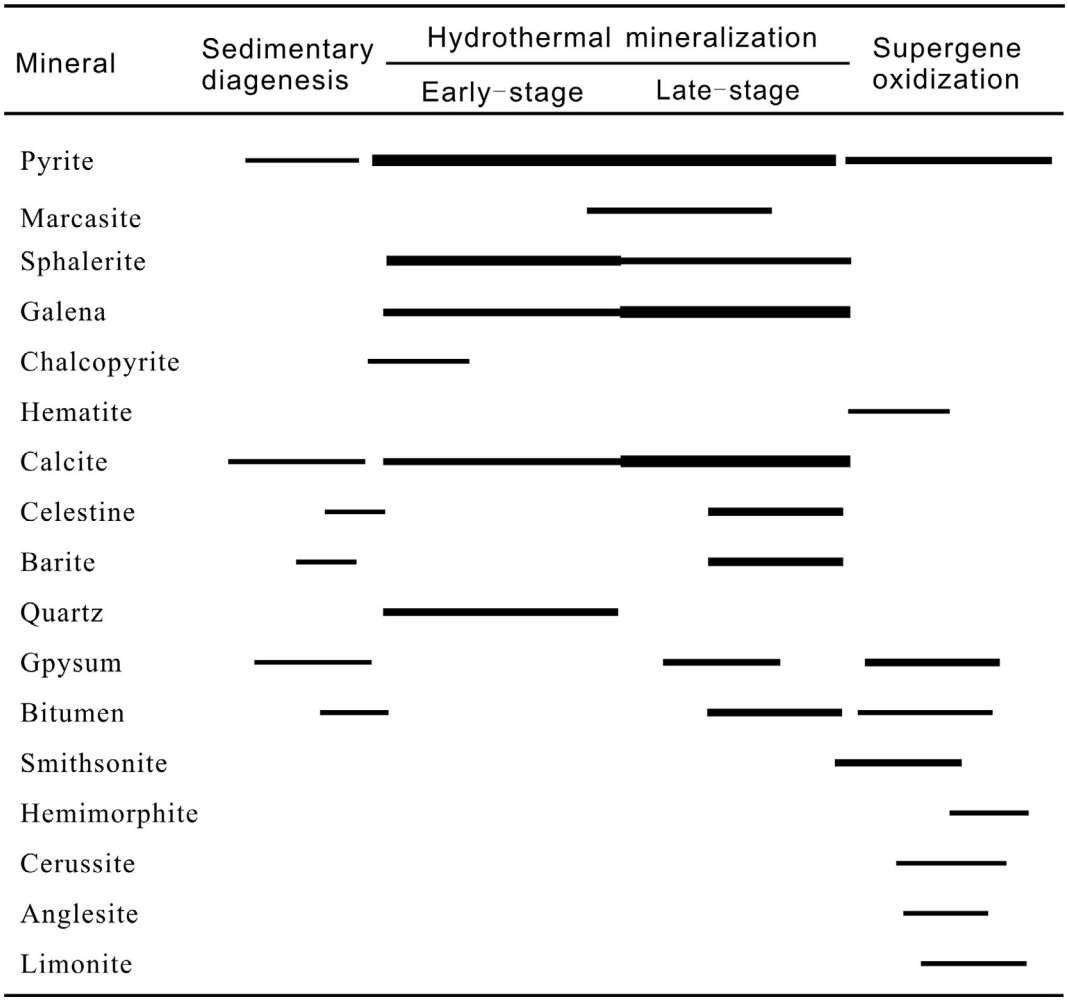

Fig. 5. Simplified paragenesis of major ore and gangue minerals in the Jinding deposit. The width of the bars represents the relative abundance of the minerals.

(Fig. 6d). Considering the paragenetic relationship between sulfate minerals and late-stage sulfides, we ascribe the positive Eu anomalies to possible micro-inclusions of sulfate minerals or to interactions between the fluid and evaporite-bearing sequences in the basin. However, the presence of moderately to weakly negative Ce anomalies suggests that the fluids interacted with sulfates derived from a marine origin, mostly likely from the Upper Triassic strata.

5.1.2. Constraint from noble gas isotopes

Because the crushing procedure is not able to separate different generations of fluid inclusions in samples, the results of the noble gas isotopic measurements represent an average of all fluid inclusions trapped in the mineral (e.g., Stuart et al., 1994). Little evidence is available to indicate significant post-modification of the He isotope compositions in the sulfide-hosted fluid inclusions of the Jinding deposit. Despite this, we cannot rule out processes such as the addition of cosmogenic ^{3}He or radiogenic ^{4}He and He diffusive loss. Because the samples were collected from an underground stope, the interference of cosmogenic ^{3}He can be largely ruled out (Foeken et al., 2009). Furthermore, significant production of ^{4}He by the decay of U and Th can be excluded due to very low concentrations of these elements in the galena, the young formation age of the deposit (30–28 Ma, discussed below) and the fact that crushing does not release radiogenic He (Stuart et al., 1994). The $^{4}He/^{40}Ar$ ratios of the galena are similar to those measured in pyrite (Hu et al., 1998), which is known to have an excellent ability to retain noble gases, suggesting that the diffusive loss of He or Ar from fluid inclusions is not significant in galena. Additionally, overprinting by *in-situ* radiogenic ^{40}Ar is proven to be negligible in potassium-free minerals (Stuart et al., 1995). Therefore, the results approximate the composition of the fluids responsible for the late-stage mineralization.

The He and Ar isotopic compositions and the $^{4}He/^{40}Ar$ ratios from the galena-hosted fluid inclusions overlap with the values measured from pyrite-hosted fluid inclusions (Fig. 7), which are considered to represent the composition of the early-stage fluids (Hu et al., 1998; and this study). The similarity of the $^{40}Ar/^{36}Ar$ to atmospheric values (298.5, Mark et al., 2011) implies that the ore-forming fluids were largely derived from atmosphere-equilibrated waters that incorporated a small contribution of excess ^{40}Ar during water-rock interaction. The values are significantly less than the values typically measured in hydrothermal fluids associated with magmatism (e.g., Hu et al., 2012; Stuart et al., 1995) and are instead consistent with the interaction of aqueous fluids with K-poor sedimentary rocks.

Volatiles from the upper mantle have $^{3}He/^{4}He$ in the range of 6–9 R_a. Helium derived from the continental crust is radiogenic in origin and characterized by $^{3}He/^{4}He$ ratios that are typically less than 0.05 R_a (Ozima and Podosek, 2002). Contemporary fluids from regions of active rifting have $^{3}He/^{4}He$ ratios that are higher than 0.05 R_a, reflecting the small but significant He contribution from volatiles released by mantle melts crystallizing deep within the crust (Oxburgh et al., 1986). The role of deep faults as conduits

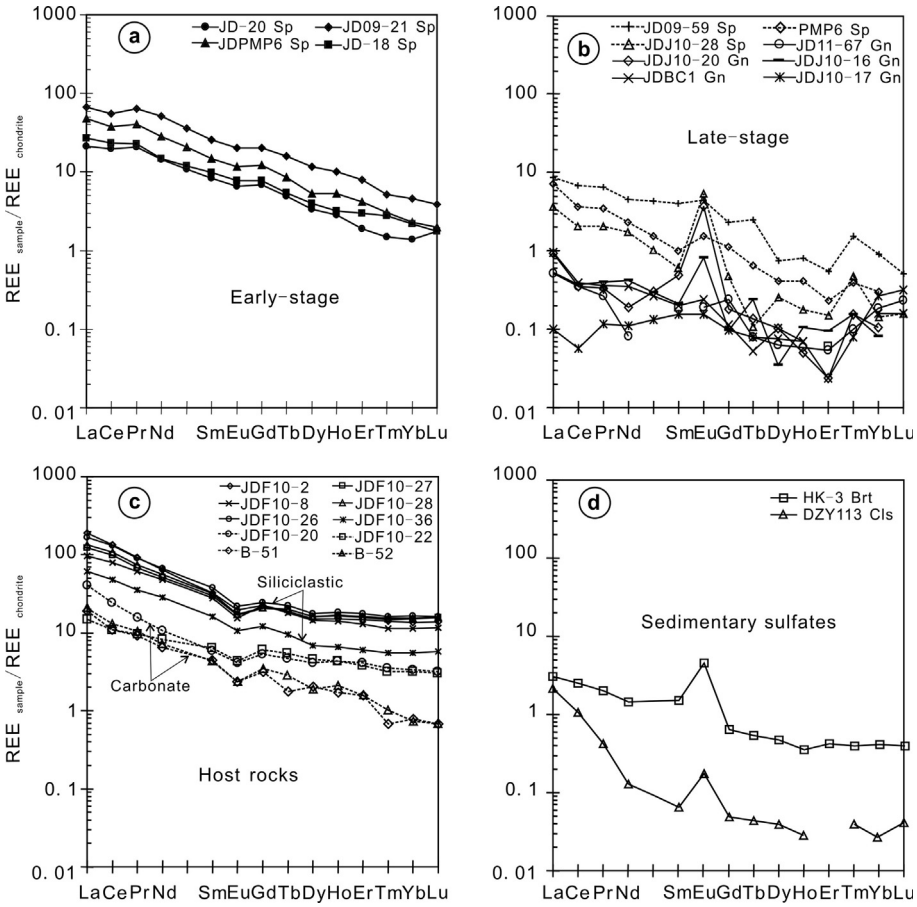

Fig. 6. Chondrite-normalized REE patterns of sulfides in the Jinding deposit in comparison with those of the host rocks and sulfate minerals in the Lanping Basin. The data used for normalization are from Sun and McDonough (1989).

Table 1
REE compositions of sulfides and host rocks from the Jinding deposit (*ppm*).

Sample no.	Description	La	Ce	Pr	Nd	Sm	Eu	Gd	Tb	Dy	Ho	Er	Tm	Yb	Lu	ΣREE	LREE/HREE	δEu	δCe
Early-stage sulfides																			
JD-20	Sphalerite	5.01	12.20	1.97	6.73	1.27	0.38	1.41	0.18	0.86	0.16	0.31	0.04	0.23	0.05	30.8	8.51	0.86	0.95
JDPMP6	Sphalerite	11.4	22.80	3.82	13.20	2.28	0.67	2.53	0.32	1.33	0.30	0.69	0.08	0.39	0.05	59.9	9.54	0.85	0.84
JD09-21	Sphalerite	15.7	33.50	6.01	23.80	3.93	1.17	4.19	0.60	2.98	0.57	1.32	0.13	0.79	0.10	94.8	7.88	0.88	0.85
JD-18	Sphalerite	6.46	14.20	2.17	6.87	1.50	0.45	1.60	0.21	1.01	0.18	0.49	0.07	0.37	0.05	35.6	7.97	0.89	0.93
Late-stage sulfides																			
PMP6	Sphalerite	1.66	2.23	0.32	1.07	0.15	0.09	0.23	0.02	0.11	0.02	0.04	0.01	0.05	–	6.00	11.6	1.45	0.70
JD09-59	Sphalerite	2.03	4.12	0.61	2.11	0.61	0.25	0.48	0.09	0.19	0.05	0.09	0.04	0.15	0.01	10.8	8.89	1.37	0.90
JDJ10-28	Sphalerite	0.85	1.25	0.20	0.80	0.09	0.31	0.10	0.00	0.07	0.01	0.03	0.01	0.02	0.00	3.73	14.5	9.86	0.72
JD11-67	Galena	0.12	0.22	0.03	0.04	–	0.01	0.05	0.00	0.02	–	0.01	–	0.03	0.01	0.53	3.58	1.59	0.90
JDJ1-20	Galena	0.22	0.21	0.03	0.09	0.08	0.21	0.04	–	0.03	–	0.00	0.00	0.02	–	0.93	9.48	10.9	0.55
JDBC1	Galena	0.23	0.24	0.03	0.17	0.03	0.01	–	–	0.03	0.00	–	–	0.03	0.00	0.77	11.3	1.53	0.60
JDJ10-17	Galena	0.02	0.04	0.01	0.05	0.02	0.01	0.02	0.00	–	0.00	0.00	–	0.05	0.01	0.24	1.85	1.22	0.53
JDJ10-16	Galena	0.13	0.23	0.04	0.20	0.03	0.05	0.02	0.01	0.01	0.01	0.02	0.00	0.01	–	0.75	8.59	5.40	0.80
Host rocks																			
JDF10-26	Siltstone, J_2h	39.4	80.7	8.57	31.2	5.80	1.27	5.06	0.84	4.48	1.04	2.90	0.41	2.82	0.41	185	9.30	0.70	1.03
JDF10-27	Siltstone, J_2h	29.1	60.6	6.49	23.8	4.58	0.97	4.17	0.75	4.10	0.94	2.61	0.38	2.57	0.40	141	7.89	0.67	1.04
JDF10-28	Siltstone, J_2h	32.0	66.5	7.09	26.0	4.87	0.99	4.27	0.75	4.12	0.96	2.66	0.40	2.63	0.40	154	8.50	0.65	1.04
JDF10-2	Sandstone, K_1j	45.3	82.2	8.76	29.5	4.94	1.14	4.58	0.70	3.81	0.86	2.42	0.36	2.28	0.35	187	11.2	0.72	0.95
JDF10-8	Sandstone, K_1j	22.8	48.4	5.84	22.4	4.26	0.90	4.62	0.67	3.64	0.79	2.13	0.29	1.93	0.29	119	7.28	0.62	1.00
JDF10-36	Sandstone,E_1y	14.4	29.6	3.36	13.4	2.45	0.61	2.49	0.35	1.75	0.37	1.00	0.14	0.94	0.15	71.0	8.89	0.75	1.01
JDF10-20	Limestone,T_3s	9.5	14.6	1.46	4.97	0.90	0.24	1.08	0.18	1.03	0.25	0.67	0.09	0.57	0.08	35.6	8.04	0.73	0.86
JDF10-22	Limestone,T_3s	3.53	6.61	0.90	3.86	0.97	0.25	1.22	0.20	1.14	0.25	0.63	0.08	0.54	0.08	20.2	3.89	0.70	0.89
B-51[1]	Dolostone,T_3s	4.39	6.48	0.89	2.96	0.66	0.14	0.64	0.07	0.50	0.10	0.26	0.02	0.13	0.02	17.3	8.74	0.73	0.65
B-52[1]	Dolostone,T_3s	4.99	7.73	0.98	3.20	0.63	0.14	0.68	0.11	0.46	0.12	0.26	0.03	0.12	0.02	19.5	9.58	0.73	0.69
Sedimentary sulfates																			
HK-3[2]	Barite	0.71	1.53	0.19	0.67	0.23	0.26	0.13	0.02	0.12	0.02	0.07	0.01	0.07	0.01	4.04	7.98	4.20	1.00
DZY113[2]	Celestine	0.50	0.65	0.04	0.06	0.01	0.01	0.01	0.00	0.01	0.00	0.00	0.00	0.00	0.00	1.29	63.50	3.02	0.84

Note: the upper case of 1 represents data from Wang and Li (1991), and 2 from Zhao (2006). "–" indicates values lower than 0.002 ppm.

Table 2
He-Ar isotopic compositions of inclusion-trapped fluids in sulfides from the Jinding deposit.

Sample no.	Host mineral	$^4He/cm^3$ STP	$^3He/cm^3$ STP	R_c/R_a	$^{40}Ar/cm^3$ STP	$^{36}Ar/cm^3$ STP	$^{40}Ar/^{36}Ar$
From IGCAS							
JD09	Galena	1.83E−06	6.97E−14	0.03	8.20E−07	2.49E−09	329
JDBC1	Galena	1.55E−07	7.18E−15	0.03	2.64E−07	7.77E−10	340
JD11-4	Galena	3.27E−07	1.25E−14	0.03	1.65E−07	5.18E−10	319
JD11-6	Galena	6.93E−07	2.89E−14	0.03	4.12E−07	1.25E−09	330
JD09-54	Galena	5.75E−07	2.23E−14	0.03	4.49E−07	1.36E−09	330
JD08	Galena	1.89E−07	8.60E−15	0.03	1.00E−06	3.35E−09	301
From SUERC							
JD1367	Galena	4.44E−07	2.17E−14	0.04			
JD11-60	Galena	2.35E−08	1.12E−15	0.01			
JD1348	Galena	2.44E−07	1.35E−14	0.04			
JD1368X	Galena	2.41E−07	1.17E−14	0.04			
JD11-14	Galena	3.16E−07	1.55E−14	0.04			
JD1328	Galena	1.98E−07	1.32E−14	0.04			
JD1356	Galena	3.13E−07	1.77E−14	0.04			
JD11-35	Galena	2.51E−07	1.15E−14	0.03			
JD1368	Galena	4.65E−07	2.37E−14	0.04			
From Hu et al., 1998							
JD14	Pyrite	5.99E−08	5.04E−15	0.06	2.18E−08	7.21E−11	301
	Pyrite	1.10E−07	6.30E−15	0.04	1.87E−08	5.71E−11	327
	Pyrite	1.70E−07	1.13E−14	0.05	4.05E−08	1.29E−10	313
JD11	Pyrite	3.86E−07	1.75E−14	0.03	2.34E−07	6.93E−10	336
	Pyrite	2.27E−07	8.42E−15	0.03	7.38E−08	1.91E−10	385
	Pyrite	6.13E−07	2.59E−14	0.03	3.07E−07	8.84E−10	347
JD15	Pyrite	7.17E−08	2.59E−15	0.03	7.72E−08	2.40E−10	653
JD17	Pyrite	5.11E−08	1.94E−15	0.03	2.63E−08	7.42E−11	354

Note: $^3He/^4He$ ratios (R_c) are expressed relative to the air ratio (R_a) of 1.4×10^{-6}.

for the migration of mantle-derived volatiles into the shallow crust may be significant (Klemperer et al., 2013). Mantle-derived He dissolved in hydrothermal fluids, trapped as inclusions in sulfide minerals (Turner and Stuart, 1992), has been extensively used to trace the contribution of mantle volatiles and heat sources in ore deposits (e.g., Davidheiser-Kroll et al., 2014; Hu et al., 2012, 2008; Stuart et al., 1995). Both the early- and late-stage ore fluids associated with the Jinding deposit possessed low $^3He/^4He$ values that approach crustal He values (Fig. 7b), implying that the He was released from crustal sources. Thus, the heat driving the circulation of hydrothermal fluids was also generated by crustal sources.

Xue et al. (2003) and Wang et al. (2004) reported consistent He-Ar isotopic data from the Jinding deposit, with $^3He/^4He$ ratios ranging from 0.19 to $1.02R_a$, 1–2 orders of magnitude higher than those of this study and Hu et al. (1998). Approximately 2–15.6% of the He in the fluids was estimated to have been derived from the mantle (Xue et al., 2003). This discrepancy can in part be explained by the analytical procedures: melting rather than crushing may release cosmogenic ^3He and air-derived He may be analyzed due to the analysis of minerals from which trapped He has diffused. Probably the main source of the discrepancy is that the analysis of He isotopes using instruments that do not adequately resolve $^3He^+$ from HD^+ isobaric interference will always overestimate the $^3He/^4He$ ratios.

5.1.3. Constraints from existing data

A large amount of data has been published in past decades on the Jinding deposit and these data could provide more constraints on the properties of the ore fluids and sources of the metals. As shown in Fig. 8, fluid inclusions from the early-stage minerals display relatively high homogenization temperatures and salinities (150–300 °C, >8 *wt% $NaCl_{eq}$*) compared to those from late-stage minerals (50-200 °C, <8 *wt% $NaCl_{eq}$*). Elevated brine temperatures are not commonly observed in MVT deposits, except in Irish Midland deposits (e.g., Wilkinson, 2010). High-temperature, saline fluids are more commonly associated with SEDEX deposits (e.g., Forrest, 1983; Leitch and Lydon, 2000), possibly due to the

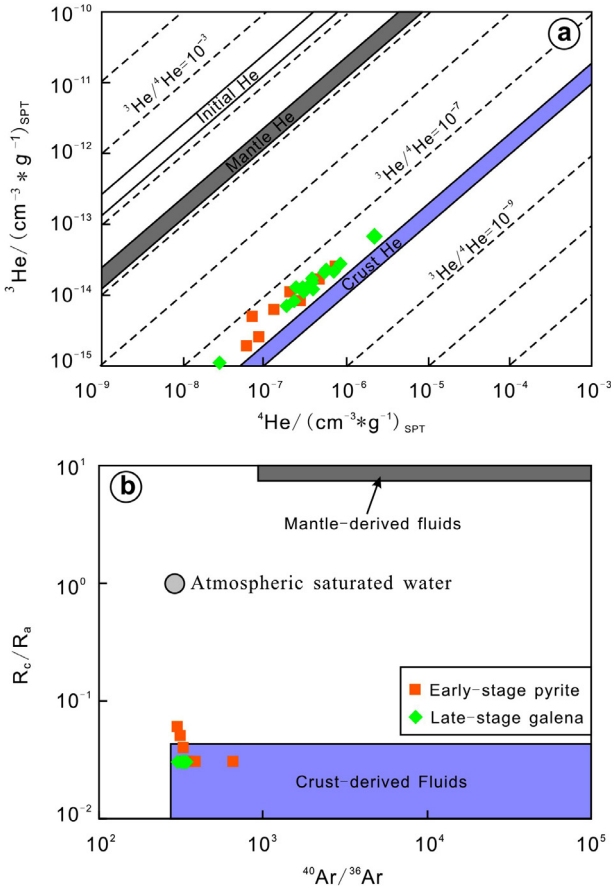

Fig. 7. Plots of ^3He vs. ^4He (a) and $^3He/^4He$ vs. $^{40}Ar/^{36}Ar$ (b) for inclusion-trapped fluids from the Jinding deposit.

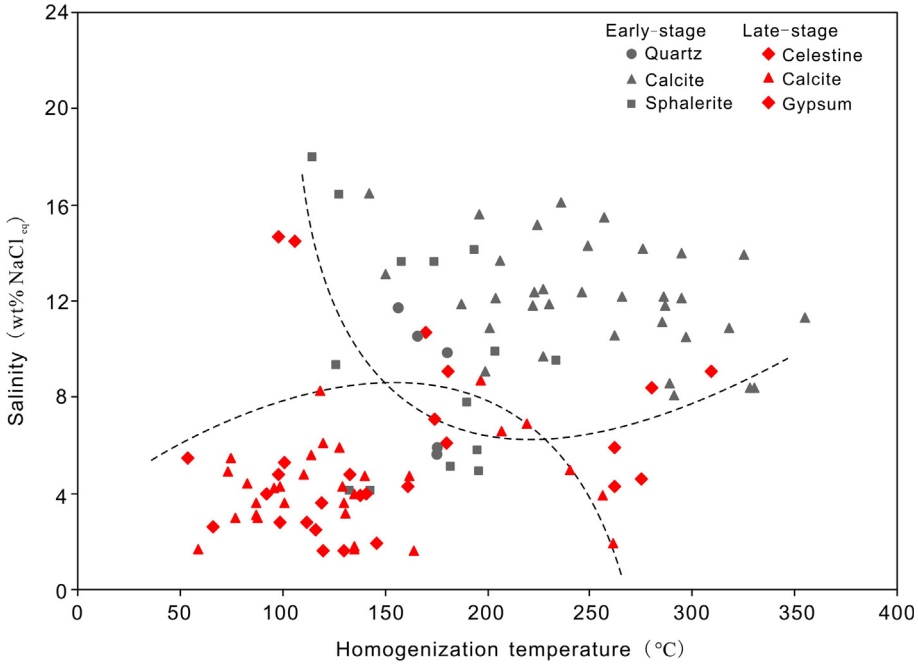

Fig. 8. Plot of homogenization temperature vs. salinity for fluid inclusions from the Jinding deposit. Data are listed in Appendix A.

unusually high geothermal gradients associated with extensional tectonism or from the circulation of the brines in the deep crust (Leach et al., 2005). Additionally, a high heat flow could be linked to contemporaneous magmatic activity, although no igneous rocks have been found near the Jinding deposit. High-salinity fluids can be formed from the dissolution of evaporite minerals, the incorporation of connate brines and/or the infiltration of evaporated surface waters (Hanor, 1979). Based on the presence of widespread evaporate-bearing red beds in the Lanping Basin, the dissolution of evaporites is the likely source of salinity in the fluids. The H and O isotope data from the fluid inclusions suggest a mixture of fluids from sedimentary rocks and primary magmatic waters for the early-stage mineralization (Fig. 9). Alternatively, the fluids could also have evolved from meteoric water that experienced strong

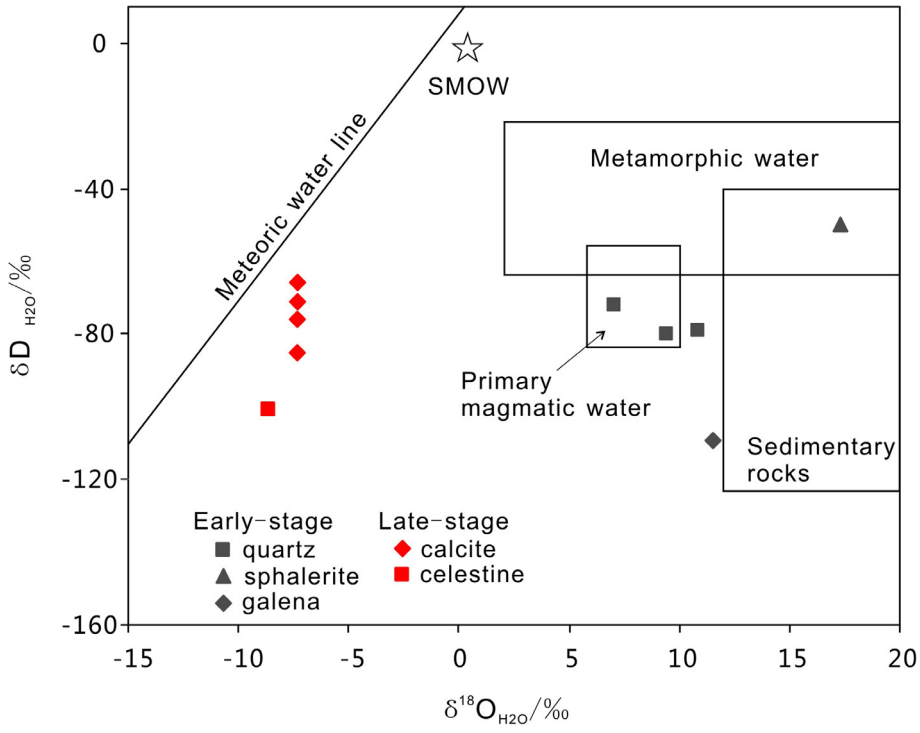

Fig. 9. Plot of δD_{H2O} vs. $\delta^{18}O_{H2O}$ values of water in the fluid inclusions from the Jinding deposit. The meteoric water line is defined as "$\delta D = 7.9\ \delta^{18}O + 8.2$" by Chen and Wang (2004). The ranges of primary magmatic and metamorphic water are calculated for water in equilibrium with normal igneous rocks at more than 700 °C and water in equilibrium with silicate minerals at 300–600 °C, respectively (Misra, 2000). The range for sedimentary rocks is depicted by Taylor (1974). Data are listed in Appendix B.

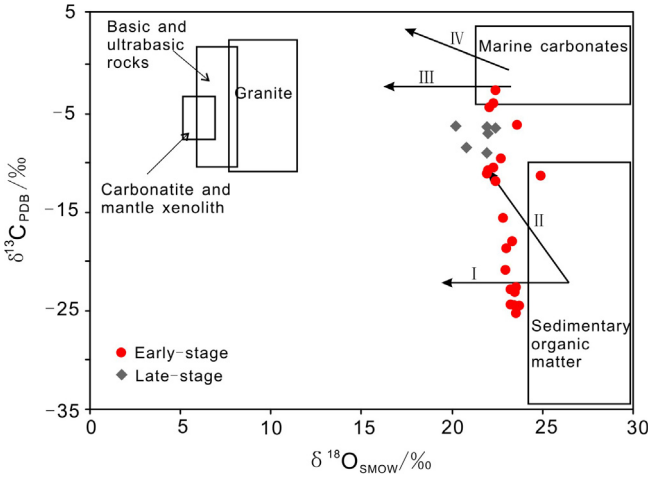

Fig. 10. Plot of $\delta^{13}C$ vs. $\delta^{18}O$ for calcites from the Jinding deposit (after Liu and Liu, 1997). I-Oxidation of sedimentary organics. II-Dehydroxylation. III-Dissolution of marine carbonate. IV-Decarboxylation. Data are listed in Appendix C.

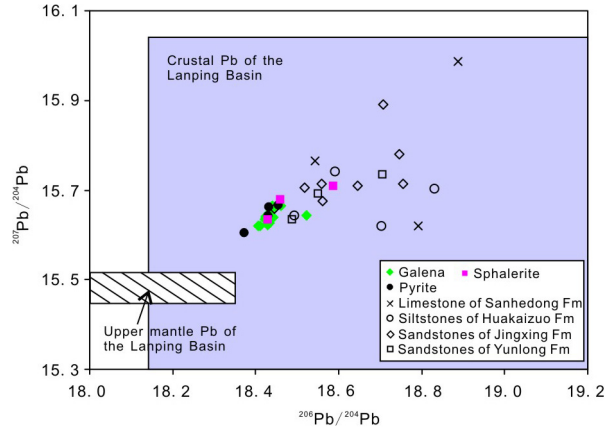

Fig. 11. Plot of $^{207}Pb/^{204}Pb$ vs. $^{206}Pb/^{204}Pb$ for sulfides from the Jinding deposit. The ranges of crustal and mantle Pb in the Lanping Basin are outlined according to (Zhang et al., 2002). Data are listed in Appendix D.

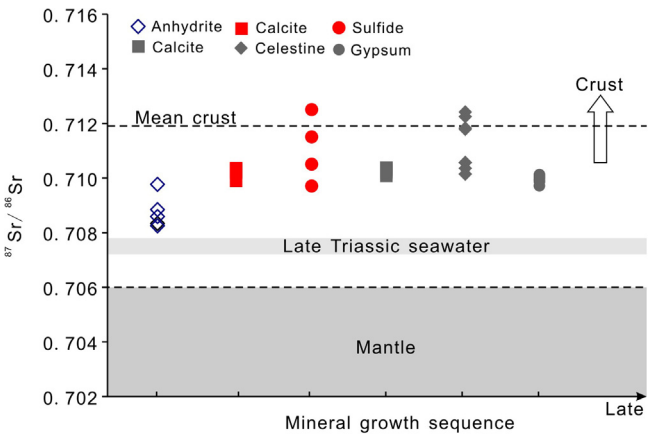

Fig. 12. The $^{87}Sr/^{86}Sr$ variations in minerals from the Jinding deposit. The range of the Sr isotopic composition of the mantle is based on Faure (1977) and that of the crust is based on Palmer and Edmond (1989). The Sr isotopic composition of Late Triassic seawater is estimated from contemporaneous marine carbonates (Korte et al., 2003; Li, 1998). Data are listed in Appendix E.

isotopic exchange with the host rocks at elevated temperatures; the δD values are approximately equivalent to those of meteoric water, but the $\delta^{18}O$ values are more similar to fluids that have interacted with sedimentary rocks. The late-stage fluids originated from meteoric water because the H and O isotopic data plot close to the meteoric water line, which also explains the lower homogenization temperatures and salinities of the fluid inclusions.

The differences between the ore fluids responsible for the early- and late-stage mineralizations are also expressed in the C and O isotopes of the associated calcite (Fig. 10). The C associated with the early-stage fluids mainly came from marine carbonates and sedimentary organic materials. Wang et al. (2009b) used biomarkers to show that the organic matter in the Jinding deposit originated from the carbonate rocks in the Triassic Sanhedong Fm. This finding is consistent with the REE and noble gas isotope data, which suggest that the early-stage fluids dissolved Triassic marine carbonates. However, the fertility of these fluids would have been dependent on later interactions with host rocks. The C isotope ($\delta^{13}C$) values in the late-stage calcite range from −9.0 to −6.2‰, suggesting that the calcite precipitated from meteoric water (Luo et al., 1994).

As stated above, no strong evidence of mantle-derived fluids exists. This finding is in accordance with the Pb and Sr isotope data. Although some previous Pb isotope data have a mantle isotope signature (Qin and Zhu, 1991; Ye et al., 1992; Zhang, 1993; Zhao, 1989), the reliability of the data has been questioned (Song et al., 2011). The Pb isotopic data published most recently suggest that the Pb was derived from a crustal source, specifically the Mesozoic-Cenozoic sedimentary rocks (Fig. 11). Lead isotopes cannot distinguish the early-stage from late-stage sulfides, which suggests that both early and late stages interacted with the same Pb source. Gangue minerals and sulfides associated with each stage of sulfide mineralization display variable $^{87}Sr/^{86}Sr$ ratios, indicating that Sr was derived from radiogenic, upper crustal aluminosilicate rocks and Upper Triassic sedimentary anhydrite precipitated from seawater (Fig. 12).

5.2. The hydrothermal mineralization processes

Although many attempts (e.g., Gao et al., 2012; Li et al., 2000; Tang et al., 2013a; Xiu et al., 2006; Xue et al., 2003; Zhang, 1993) have been made to date the formation of the Jinding deposit, none of the data obtained so far are considered to represent the age of mineralization. The lack of precise and accurate ages hinders our understanding of the complex processes involved in the formation of the Jinding mineral deposit and our ability to establish a reasonable genetic model. As the deposit is spatially controlled by the nappe thrust faults and occurs within a tectonic dome associated with regional overthrusting (Wu and Wu, 1989), the mineralization should have formed during or immediately after the overthrusting (~37 Ma), but before the latest tectonothermal event (25.8–35.9 Ma) revealed by the apatite fission track ages (Li et al., 2000). Wang et al. (2009a) further restricted the age of the deposit to 33–28 Ma, in accordance with the timing (37–27 Ma) of other Pb-Zn mineralization in the Lanping region and its analogous basins (e.g., Tuotuohe and Changdu) (Jiang et al., 2014; Li et al., 2000; Song et al., 2011; Tian et al., 2009; Wang et al., 2011; Zou et al., 2015). These data suggest that the Jinding deposit likely formed as a result of large-scale regional hydrothermal activity during the late collisional stage (41–26 Ma) of the India-Asia collision (Hou et al., 2006).

Following the Middle Triassic, the Lanping region evolved into a rift basin, with the development of hydrothermal rocks accompanied by alkaline-associated mineralization (Zhang et al., 2010). Following rifting, thick evaporite-bearing red beds intercalated with organic matter-rich fine clastic layers were deposited during the

Middle Jurassic. The occurrence of organic matter caused local basinal fluids to become reducing, which favored the deposition of numerous ore minerals (Zhao, 2006). The associated strata have relatively high concentrations of Pb, Zn, Cu, Ag, Ba, Co and Ni, which provide favorable source rocks for the Cenozoic base metal mineralization in the region (Ye et al., 1992).

Our REE results highlight the roles of marine carbonates and evaporite sequences in the formation of the ore fluids, along with the strong interactions with the host rocks. The He isotopic data exclude a mantle origin for the fluids associated with the Jinding deposit, similar to the He isotope results from Cu deposits ($^3He/^4He$ = 0.01–0.06 R_a, Zhang et al., 2015) and Ag-Cu-Pb-Zn polymetallic deposits ($^3He/^4He$ = 0.01–0.14 R_a, Zou, 2013) in the western basin. The involvement of mantle-derived fluids is apparently not necessary for the formation of sediment-hosted giant base metal deposits; rather, other factors associated with the efficient precipitation of ore metals, such as the dominance of bacteriogenic sulfur (Tang et al., 2014), are likely key to developing economic accumulations of ore similar to the Nanvan deposit (Davidheiser-Kroll et al., 2014).

Compression associated with the initial collision of Indian and Asian continents in the Early Paleocene caused the development of large-scale overthrusting (the Jinding dome probably formed during this period) and the juxtaposition of Mesozoic rocks over Cenozoic strata (He et al., 2009). Strong tectonic activity might have led to the activation of organic matter and migration to favorable traps, such as the Jinding dome. This hypothesis is supported by the bitumen Re-Os isochron age of 68 Ma (Gao et al., 2012), which further suggests that the formation of an oil and gas reservoir created excellent conditions for sulfide precipitation because it not only contained considerable bacteriogenic sulfur but also provided the hydrocarbons necessary to reduce dissolved sulfates. An *in-situ* sulfur isotope study revealed that the sulfur associated with the precipitation of the early-stage sulfides was largely derived from bacteriogenic reduction, in contrast to that of the late-stage sulfides which might have been associated with thermochemically sulfate reduction (Tang et al., 2014).

Due to the oblique compression associated with the continuous convergence of the Indian and Asian continents in the Eocene to Early Oligocene, the Lanping basin was modified by strong strike-slip faulting (He et al., 2009; Hou et al., 2006). On-going compression might have caused the dehydration of aquifers (e.g., aquifers in Upper Triassic carbonates) and the release of metals from the roots of the thrust nappe systems, thereby allowing these metals to migrate upward along the gently-dipping detachment zones (Hou et al., 2008). The fluids were enriched in metals and ligands due to interactions with the host rocks and eventually evolved into hot metalliferous basinal brines, which would have precipitated ore minerals when they encountered reduced sulfur (H_2S) in an oil-rich reservoir within the Jinding dome. The fine-grained textures of the early-stage sulfides were in agreement with rapid precipitation. The ore fluids associated with the late-stage mineralization were derived from meteoric waters, which might have acquired metals from the evaporite-bearing sequences during infiltration. For example, the Upper Triassic anhydrite-bearing rocks containing high concentrations of Pb (19–42 ppm) and Sr (914–4535 ppm) are suggested to have released metals into the ambient cool fluids during dissolution (Gao, 1991). Additionally, the increase in sulfate anions in the late-stage fluid inclusions (Luo et al., 1994; Wen et al., 1995) and the presence of sulfate minerals suggest that the late-stage fluids were also likely rich in sulfates. These dissolved sulfates would have been thermochemically reduced by hydrocarbons, leading to the precipitation of late-stage sulfides.

6. Conclusions

The early-stage sulfides in the Jinding deposit have relatively high ∑REE values and weakly negative Ce anomalies, suggesting that the formation of the associated fluids involved the dissolution of Upper Triassic marine carbonates with the input of REEs from aluminosilicate rocks in the basin. In contrast, the late-stage sulfides have irregular REE patterns and positive Eu anomalies, indicating evaporite-bearing strata were the source of the REEs. The noble gas isotopic data produced in this study are consistent with those of Hu et al. (1998), and they reveal typical crustal $^3He/^4He$ values and a small amount of excess ^{40}Ar, suggesting that the fluids associated with both stages of mineralization likely equilibrated with surface waters without discernible mantle-derived components. This conclusion agrees with fluid inclusion data and H, O, C, S, Pb and Sr isotope data, which support crustal origins for the fluids, despite the differences in the precipitation mechanisms between the mineralization stages.

Acknowledgements

The research was jointly funded by the National Basic Research Program (2015CB452603), NSERC Discovery Grant to Fayek, China Scholarship Council (201404910273), Institute of Geochemistry, Chinese Academy of Sciences (Y5CJ002000 and 201401), Natural Science and Technology Fund of Guizhou Province (Y5DF110000) and Strategy Survey Program of the Tri-Rare Metal Resources of China (12120113078200). We thank two anonymous reviewers and Prof. Qingfei Wang and Franco Pirajno for their constructive comments, which greatly contribute to improvement of this manuscript.

Appendix

Appendix A
Homogenization temperatures and salinities of the fluid inclusions.

Host mineral	Th/°C	Sal/*wt% $NaCl_{eq}$*	Host	Th/°C	Sal/*wt% $NaCl_{eq}$*
Early-stage mineralization			Late-stage mineralization		
Quartz (Xue et al., 2007)	181	9.8	Calcite	140	4.7
	176	5.6	(Xue et al., 2007)	162	4.7
	176	5.9		256	3.9
	166	10.5		240	5.0
	157	11.7		135	4.0
Sphalerite (Xue et al., 2007)	234	9.5		135	1.8
	204	9.9		87	3.6
	174	13.6		87	3.1

(*continued on next page*)

Appendix A (*continued*)

Host mineral	Th/°C	Sal/*wt% $NaCl_{eq}$*	Host	Th/°C	Sal/*wt% $NaCl_{eq}$*
	195	5.8		101	3.6
	196	4.9		99	4.3
	190	7.8		77	3.0
	182	5.1		75	5.5
	194	14.1		120	6.1
	143	4.1		83	4.4
	133	4.1		73	4.9
	128	16.4		59	1.7
	126	9.3		88	3.0
	158	13.6	Calcite (Tang et al., 2011)	240	3.2
	115	18.0		219	6.9
Calcite (Tang et al., 2011)	295	12.1		207	6.6
	287	11.8		118	8.3
	286	12.2		197	8.7
	262	10.6		164	1.6
	266	12.2		261	1.9
	276	14.2		96	4.2
	227	9.7	Celestine (Xue et al., 2007)	181	9.1
	246	12.4		170	10.7
	249	14.3		133	4.8
	230	11.9		309	9.1
	257	15.5		275	4.6
	222	11.8		262	5.9
	227	12.5		280	8.4
	199	9.1		262	4.3
	223	12.4		106	14.5
	201	10.9		161	4.3
	204	12.1		174	7.1
	236	16.1		180	6.1
	224	15.2		120	1.6
	206	13.7		119	3.6
	187	11.9		146	1.9
	196	15.6		98	14.7
	150	13.1	Gypsum (Xue et al., 2007)	98	4.8
	142	16.5		66	2.6
Late-stage mineralization				54	5.5
				141	4.0
Calcite (Xue et al., 2007)	131	3.2		138	3.9
	135	1.7		92	4.0
	130	3.6		101	5.3
	129	4.3		99	2.8
	110	4.8		112	2.8
	128	5.9		116	2.5
	114	5.6		130	1.6

Note: Th-homogenization temperature, Sal-salinity.

Appendix B
Hydrogen and oxygen isotopic compositions of the fluid inclusions.

Sample no.	Host mineral	Relative to SMOW (‰)	
		δD_{H2O}	$\delta^{18}O_{H2O}$
Early-stage (Ye et al., 1992; Zhao, 1989)			
JB1474	Calcite	−65.7	−7.31
JB1443	Calcite	−70.9	−7.31
JB1450	Calcite	−75.9	−7.31
JB1449	Calcite	−85.3	−7.31
	Celestine	−100.6	−8.64
Late-stage (Ye et al., 1992; Zeng, 2007)			
BTW1	Sphalerite	−50.1	17.27
BTW8	Galena	−109.3	11.56
JY15	Quartz	−72	6.98
JY16	Quartz	−80	9.4
JY17	Quartz	−79	10.78

Appendix C
Carbon and oxygen isotopic compositions of the hydrothermal calcites.

Sample no.	$\delta^{13}C_{PDB}$ (‰)	$\delta^{18}O_{SMOW}$ (‰)
Early-stage (Li, 1998; Luo et al., 1994; Tang et al., 2011)		
PBT1	−20.9	23.6
JPTW3	−6.1	23.6

Appendix C (*continued*)

Sample no.	$\delta^{13}C_{PDB}$ (‰)	$\delta^{18}O_{SMOW}$ (‰)
JPTW4	−18	23.3
Ty207	−24.5	23.7
Ty208	−24.4	23.2
Ty209	−11.9	22.4
JB1436	−24.5	23.4
JD09-15	−23	23.4
JD09-45	−22.6	23.5
JDJ10-22	−15.6	22.8
JDF10-22-1	−3.9	22.3
JDJ10-27	−4.3	22.1
JDJ10-37	−2.6	22.4
Jia07	−18.6	23.0
360-11b	−25.2	23.5
360-11c	−22.8	23.2
C2633-07b	−11.1	21.9
2633-04	−10.5	22.3
2633-G	−10.8	22.0
175-16	−9.6	22.7
175-27	−11.3	24.9
Late-stage (Li, 1998; Tang et al., 2011)		
JDJ10-15A	−6.2	20.2
JDJ10-13	−7.0	22.0
JDJ10-40	−6.5	22.4
C2633-13	−8.4	20.8
C2633-31a	−9.0	21.9
C2633-16	−6.4	21.9

Appendix D
Lead isotopic compositions of the sulfides.

Sample no.	Mineral	$^{206}Pb/^{204}Pb$	$^{207}Pb/^{204}Pb$	$^{208}Pb/^{204}Pb$	References
JDPMP6	Galena	18.407	15.621	38.567	Tang et al., 2013b
JDF10-13	Galena	18.424	15.642	38.631	
JD09-54	Galena	18.460	15.665	38.713	
JD-05	Galena	18.429	15.622	38.576	
JDBC3	Galena	18.429	15.624	38.578	
JDJ10-17	Galena	18.443	15.661	38.694	
JX17	Galena	18.410	15.620	38.569	Wang et al., 2009a
JX18	Galena	18.425	15.640	38.634	
JX27	Galena	18.523	15.643	38.623	
JG30	Galena	18.434	15.626	38.599	
JG32-1	Galena	18.442	15.639	38.638	
JX135	Galena	18.436	15.653	38.677	
JX165	Galena	18.436	15.649	38.666	
JX251-3	Galena	18.421	15.634	38.616	
JDJ1-5	Galena	18.452	15.665	38.711	Zhao, 2006
PMP1-2	Galena	18.440	15.664	38.703	
PMP1-1	Galena	18.437	15.663	38.696	
JD09-21	Sphalerite	18.428	15.634	38.618	Tang et al., 2013b
JD-05	Sphalerite	18.429	15.634	38.612	
JX27	Sphalerite	18.586	15.709	38.821	Wang et al., 2009a
JX251-8	Sphalerite	18.458	15.679	38.765	
JX93	Pyrite	18.444	15.658	38.693	
JD09-12	Pyrite	18.373	15.605	38.524	Tang et al., 2013a
JD09-45	Pyrite	18.430	15.643	38.640	
JDJ1-9	Pyrite	18.454	15.668	38.726	Zhao, 2006
PMP1-5	Pyrite	18.432	15.663	38.700	
No.3	Limestone T_3s	18.544	15.765	38.915	Zhao, 1989
No.5	Limestone T_3s	18.888	15.988	39.464	
1	Limestone T_3s	18.791	15.619	38.611	Luo et al., 1994
2	Limestone T_3s	19.204	15.772	38.957	
LP08-67-1	Siltstone J_2h	18.492	15.644	38.564	Wang, 2010
LP08-67-2	Siltstone J_2h	18.830	15.703	39.322	
LP08-67-3	Siltstone J_2h	18.702	15.619	38.861	
JB308	Siltstone J_2h	18.592	15.742	39.306	Zhao, 1989
DXQ16	Sandstones K_1j	18.756	15.713	39.328	Third Geological Team, 1984
DXQ18	Sandstones K_1j	18.645	15.710	38.912	
DXQ21	Sandstones K_1j	18.560	15.714	38.924	
TJY-14	Sandstones K_1j	18.746	15.779	39.198	
J5B91	Sandstones K_1j	18.562	15.676	38.854	
No.1	Sandstones K_1j	18.517	15.705	38.888	Zhao, 1989
No.2	Sandstones K_1j	18.707	15.891	39.317	

(*continued on next page*)

Appendix D (*continued*)

Sample no.	Mineral	$^{206}Pb/^{204}Pb$	$^{207}Pb/^{204}Pb$	$^{208}Pb/^{204}Pb$	References
JB439	Sandstones E_1y	18.488	15.636	38.632	
JB453-1	Sandstones E_1y	18.549	15.693	38.809	
1	Sandstones E_1y	18.706	15.736	38.934	Luo et al., 1994
2	Sandstones E_1y	18.488	15.636	38.632	
3	Sandstones E_1y	18.549	15.693	38.809	

Appendix E
Strontium isotopic compositions of the minerals.

Sample	Mineral	$^{87}Sr/^{86}Sr$	References
19-03	Anhydrite	0.708283	Li, 1998
19-05	Anhydrite	0.708231	
19-06	Anhydrite	0.708543	
338-01	Anhydrite	0.708825	
101-20	Anhydrite	0.709726	
259-363.7	Gypsum	0.710042	
259-01	Gypsum	0.710021	
145-13	Gypsum	0.709842	
23-01	Gypsum	0.70996	
19-02	Gypsum	0.710094	
129-12	Gypsum	0.709703	
338-07	Gypsum	0.709852	
JD09-15	Calcite	0.71026	Tang et al., 2013b
JD09-45	Calcite	0.71019	
JDJ10-22	Calcite	0.71036	
JDJ10-27	Calcite	0.70986	
JDJ10-37	Calcite	0.71016	
JDJ10-15A	Calcite	0.71028	
JDJ10-40	Calcite	0.71024	
Jia07	Calcite	0.7102	Li, 1998
360-11b	Calcite	0.71021	
360-11c	Calcite	0.71022	
C2633-07b	Calcite	0.71022	
C2633-04	Calcite	0.710235	
2633-G	Calcite	0.710257	
175-16	Calcite	0.710276	
175-27	Calcite	0.71028	
C2633-13	Calcite	0.71033	
C2633-31a	Calcite	0.71035	
C2633-16	Calcite	0.71035	
JY-03	Celestine	0.710553	Hu et al., 2013
JY-06	Celestine	0.710352	
03_9_20	Celestine	0.71011	
03_9_21	Celestine	0.710133	
Sr5	Celestine	0.71057	Luo et al., 1994
JD-B-P25(Sr1)	Celestine	0.71185	
JD-B-P25(Sr2)	Celestine	0.71177	
BTW5	Celestine	0.71243	
BTW6	Celestine	0.71055	
JDJ-2	Sulfide	0.711479	Hu et al., 2013
JDJ-3	Sulfide	0.712258	
JDJ-6	Sulfide	0.710412	
JDB-2	Sulfide	0.709798	

References

Bai, J.F., Wang, C.H., Na, R.X., 1985. Geological characteristics of the Jinding lead-zinc deposit in Yunnan with a special discussion on its genesis. Miner. Deposits 4, 1–9 (in Chinese with English abstract).

Bau, M., Dulski, P., 1999. Comparing yttrium and rare earths in hydrothermal fluids from the Mid-Atlantic Ridge: implications for Y and REE behavior during near-vent mixing and for the Y/Ho ratio of Proterozoic seawater. Chem. Geol. 155, 77–90.

Bau, M., Moller, P., 1992. Rare earth element fractionation in metamorphogenic hydrothermal calcite, magnesite and siderite. Miner. Petrol. 45, 231–246.

Bau, M., Romer, R.L., Luders, V., Dulski, P., 2003. Tracing element sources of hydrothermal mineral deposits: REE and Y distribution and Sr-Nd-Pb isotopes in fluorite from MVT deposits in the Pennine Orefield, England. Miner. Deposita 38, 992–1008.

Bilal, B.A., Müller, E., 1992. Thermodynamic study of Ce4+/Ce3+ redox reaction in aqueous solutions at elevated temperatures. 1. Reduction potential of Ce4+ in perchloric acid solution. Phys. Sci. 47, 231–246.

Chen, J., Wang, H.N., 2004. Geochemistry. Science Press, Beijing.

Davidheiser-Kroll, B., Stuart, F.M., Boyce, A.J., 2014. Mantle heat drives hydrothermal fluids responsible for carbonate-hosted base metal deposits: evidence from 3He/4He of ore fluids in the Irish Pb-Zn ore district. Miner. Deposita 49, 547–553.

Deng, J., Wang, Q.F., Li, G.J., 2016. Superimposed orogeny and composite metallogenic system: case study from the Sanjiang Tethyan belt, SW China. Acta Petrol. Sinica 32, 2225–2247 (in Chinese with English abstract).

Deng, J., Wang, Q.F., Li, G.J., Li, C.S., Wang, C.M., 2014. Tethys tectonic evolution and its bearing on the distribution of important mineral deposits in the Sanjiang region, SW China. Gondwana Res. 26, 419–437.

Douville, E., Bienvenu, P., Charlou, J.I., 1999. Yttrium and rare earth elements in fluids from various deep-sea hydrothermal systems. Geochem. Cosmochem. Acta 63, 627–643.

Faure, G., 1977. Principles of Isotope Geology. John Wiley & Sons Inc, New York.

Foeken, J.P.T., Day, S., Stuart, F.M., 2009. Cosmogenic 3He exposure dating of the Quaternary basalts from Fogo, Cape Verdes: implications for rift zone and magmatic reorganisation. Quatern. Geochron. 4, 37–49.

Forrest, K., 1983. Geological and isotopic studies of the Lik deposit and the surrounding mineral district, DeLong Mountains, western Brooks Range, Alaska (Ph.D Thesis). University of Minnesota, Minneapolis (161 pp.).

Fu, X.G., 2005. Evolution of the Lanping basin and formation of relevant metal deposits. J. Earth Sci. Environ. 27, 26–32 (in Chinese with English abstract).

Gao, B.Y., Xue, C.J., Chi, G.X., Li, C., Qu, W.J., Du, A.D., Li, Z.X., Gu, H., 2012. Re-Os dating of bitumen in the giant Jinding Zn-Pb deposit, Yunnan and its geological significance. Acta Petrol. Sinica 28, 1561–1567 (in Chinese with English abstract).

Gao, G.L., 1991. Formation age and involved problems on anhydrite ore in Jinding lead-zinc ore area. Yunnan Geol. 10, 191–206 (in Chinese with English abstract).

Hanor, J.S., 1979. The sedimentary genesis of hydrothermal fluids. In: Barnes, H.L. (Ed.), Geochemistry of Hydrothermal Ore Deposits. Wileyinterscience, New York, pp. 137–142.

He, L.Q., Song, Y.C., Chen, K.X., Hou, Z.Q., Yu, F.M., Yang, Z.S., Wei, J.Q., Li, Z., Liu, Y.C., 2009. Thrust-controlled, sediment-hosted, Himalayan Zn-Pb-Cu-Ag deposits in the Lanping foreland fold belt, eastern margin of Tibetan Plateau. Ore Geol. Rev. 36, 106–132.

Hou, Z.Q., Pan, G.T., Wang, A.J., Mo, X.X., Tian, S.H., Sun, X.M., Ding, L., Wang, E.Q., Gao, Y.F., Xie, Y.F., Zeng, P.S., Qin, K.Z., Xu, J.F., Qu, X.M., Yang, Z.M., Yang, Z.S., Fei, H.C., Meng, X.J., Li, Z.Q., 2006. Metallogenesis in Tibetan collisional orogenic belt: II. Mineralization in late-collisional transformation setting. Miner. Deposits 25, 521–543 (in Chinese with English abstract).

Hou, Z.Q., Song, Y.C., Li, Z., Wang, Z.L., Yang, Z.M., Yang, Z.S., Liu, Y.C., Tian, S.H., He, L. Q., Chen, K.X., Wang, F.C., Zhao, C.X., Xue, W.Z., Lu, H.F., 2008. Thrust-controlled, sediment-hosted Pb-Zn-Ag-Cu deposits in eastern and northern margins of Tibetan orogenic belt: geological features and tectonic model. Miner. Deposits 27, 123–144 (in Chinese with English abstract).

Hou, Z.Q., Zaw, K., Pan, G., Mo, X., Xu, Q., Hu, Y., Li, X., 2007. Sanjiang Tethyan metallogenesis in S.W. China: tectonic setting, metallogenic epochs and deposit types. Ore Geol. Rev. 31, 48–87.

Hu, G.Y., Li, Y.H., Zeng, P.S., 2013. The role of halosalt in mineralization of the Jinding Pb-Zn deposit: evidence from sulfur and strontium isotopic compositions. Acta Geol. Sinica 11, 1695–1702 (in Chinese with English abstract).

Hu, R.Z., Bi, X.W., Jiang, G.H., Chen, H.W., Peng, J.T., Qi, Y.Q., Wu, L.Y., Wei, W.F., 2012. Mantle-derived noble gases in ore-forming fluids of the granite-related Yaogangxian tungsten deposit, Southeastern China. Miner. Deposita 47, 623–632.

Hu, R.Z., Bi, X.W., Zhou, M.F., Peng, J.T., Su, W.C., Liu, S., Qi, H.W., 2008. Uranium metallogenesis in South China and Its relationship to crustal extension during the cretaceous to tertiary. Econ. Geol. 103, 583–598.

Hu, R.Z., Turner, G., Burnard, P.G., Zhong, H., Ye, Z.J., Bi, X.W., 1998. Helium and argon isotopic geochemistry of Jinding superlarge Pb-Zn deposit. Sci. China (Series D) 41, 442–448.

Jiang, B., Deng, J., Zhang, C.Q., 2014. Sediment-hosted lead-zinc deposits in Sanjiang region, SW China: characteristics and regional metallogeny. Acta Geol. Sinica 88, 2532–2544 (In Chinese with English abstract).

Klemperer, S.L., Kennedy, B.M., Sastry, S.R., Makovsky, Y., Harinarayana, T., Leech, M. L., 2013. Mantle fluids in the Karakoram fault: helium isotope evidence. Earth Planet. Sci. Lett. 366, 59–70.

Korte, C., Kozur, H.W., Bruckschen, P., Veizer, J., 2003. Strontium isotope evolution of Late Permian and Triassic seawater. Geochim. Cosmochim. Acta 67, 47–62.

Leach, D.L., Sangster, D.F., Kelley, K.D., Larger, R.R., Garven, G., Allen, C.R., Gutzmer, J., Walters, S., 2005. Sediment-hosted zinc-lead deposits: A global perspective. Economic Geology 100th Anniversery volumn, 561–607.

Leach, D.L., Song, Y.C., Hou, Z.Q., 2016. The world-class Jinding Zn–Pb deposit: ore formation in an evaporite dome, Lanping Basin, Yunnan, China. Miner. Deposita, 1–16.
Leitch, C.H.B., Lydon, J.W., 2000. Fluid inclusion petrography and microthermometry of the Sullivan deposit and surrounding area. Geological Association of Canada, Mineral Deposit Division Special Volume 1, 617–632.
Li, N., 1998. Depositional controls and genesis of the Jinding sandstonehosted Zn-Pb deposit, Yunnan province, southwest China (Ph.D Thesis). University of Texas, Austin, pp. 1-100.
Li, F., Fu, W.M., Yan, W., 1995. The REE geochemistry of strata and Cu deposit in Lanping-Simao basin. Yunnan Geol. 14, 1–12 (in Chinese with English abstract).
Li, X.M., Tan, K.X., Gong, W.J., Gong, G.L., 2000. Study on the metallogenic epoch of the Jinding lead-zinc deposit with apatite fission track analysis. Geotectonica et Metallogenia 24, 282–286 (in Chinese with English abstract).
Liao, Z.T., Chen, Y.K., 2005. Nature and evolution of Lanping-Simao basin prototype. J. Tongji Univ. 33, 1528–1531 (in Chinese with English abstract).
Liu, Y.C., Hou, Z.Q., Yang, Z.S., Tian, S.H., Song, Y.C., Yu, Y.S., Ma, W., 2016. Geology and chronology of the Zhaofayong carbonate-hosted Pb-Zn ore cluster: Implication for regional Pb-Zn metallogenesis in the Sanjiang belt, Tibet. Gondwana Res. 35, 15–26.
Liu, Y.C., Hou, Z.Q., Yu, Y.S., Tian, S.H., Li, Y.L., Yang, Z.S., 2013. Characteristics and genesis of Lalongla MVT-like deposit in Changdu region, Tibet. Acta Petrol. Sinica 29, 1407–1426 (In Chinese with English abstract).
Liu, J.M., Liu, J.J., 1997. Basin fluid genetic model of sediment-hosted microdisseminated gold deposits in the gold-triangle area between Guizhou, Guangxi and Yunnan. Acta Miner. Sinica 17, 448–456 (in Chinese with English abstract).
Luo, J.L., Yang, Y.H., Zhao, Z., Chen, J.S., Yang, J.Z., 1994. Evolution of the Tethys in Western Yunnan and Mineralization for Main Metal Deposits. Geological Publishing Press, Beijing, pp. 157-215 (in Chinese).
Lv, B.X., Qian, X.G., 1999. Petrological study of deep-derived xenoliths of Cenozoic alkaline volcanic rocks and alkali-rich porphyry rocks in western Yunnan Province. Yunnan Geol. 18, 127–143 (in Chinese with English abstract).
Mark, D.F., Rice, C.M., Fallick, A.C., Trewin, N.H., Lee, M.R., Boyce, A., Lee, J.K.W., 2011. 40Ar/39Ar dating of hydrothermal activity, biota and gold mineralization in the Rhynie hot-spring system, Aberdeenshire, Scotland. Geochim. Cosmochim. Acta 75, 555–569.
Mills, R.A., Elderfield, H., 1995. Rare earth element geochemistry of hydrothermal deposits from the active TAG Mound, 26°N Mid-Atlantic Ridge. Geochem. Cosmochem. Acta 59, 3511–3524.
Misra, K., 2000. Understanding Mineral Deposits. Kluwer Academic Publishing House, London, p. 845.
Mo, X.X., Deng, J.F., Lu, F.X., 1994. Volcanism and the evolution of Tethy in Sanjiang area, southwestern China. J. Southeast Asian Earth Sci. 9, 325–333.
Mou, C.L., Wang, J., Yu, Q., Zhang, L.S., 1999. The evolution of the sedimentary basin in the Lanping area during Mesozoic-Cenozoic. J. Miner. Petrol. 19, 30–36 (in Chinese with English abstract).
Mu, C.L., Wang, J., Yu, Q., Zhang, L.S., 1999. The evolution of the sedimentary basin in Lanping area during Mesozoic-Cenozoic. Miner. Petrol. 19, 30–36 (in Chinese with English abstract).
Oxburgh, E., O'nions, R., Hill, R., 1986. Helium isotopes in sedimentary basins. Nature 324, 632–635.
Ozima, M., Podosek, F.A., 2002. Noble Gas Geochemistry. Cambridge University Press, Cambridge.
Palmer, M.R., Edmond, J.M., 1989. The strontium isotope budget of the modern ocean. Earth Planet. Sci. Lett. 92, 11–26.
Pan, G.T., Xu, Q., Hou, Z.Q., Wang, L.Q., Du, D.X., Mo, X.X., Li, D.M., Wang, M.J., Jiang, X.S., Hu, Y.Z., 2003. The Ore-forming System of the Orogenic Processing in the Western "Sangjiang" Ploy-arc and the Resources Estimate. Geological Publishing House, Beijing.
Qi, L., Conrad, D.G., 2000. Determination of trace elements in twenty six Chinese geochemistry reference materials by inductively coupled plasma-mass spectrometry. Geostand. Newslett. 24, 51–63.
Qin, G.J., Zhu, S.Q., 1991. The ore-forming model of the Jinding lead-zinc deposit and prediction. Yunnan Geol. 10, 145–190 (in Chinese with English abstract).
Song, Y.C., Hou, Z.Q., Yang, T.N., Zhang, H.R., Yang, Z.S., Tian, S.H., Liu, Y.C., Wang, X. H., Liu, Y.X., Xue, C.D., Wang, G.H., Li, Z., 2011. Sediment-hosted Himalayan base metal deposits in Sanjiang region: characteristics and genetic types. Acta Peteol. Mineral. 30, 355–380 (in Chinese with English abstract).
Stuart, F.M., Burnard, P.G., Taylor, R.P., Turner, G., 1995. Resolving mantle and crustal contributions to ancient hydrothermal fluids: He-Ar isotopes in fluid inclusions from Dae Hwa W-Mo mineralisation, South Korea. Geochim. Cosmochim. Acta 59, 4663–4673.
Stuart, F.M., Turner, G., Duckworth, R.C., Fallick, A.E., 1994. Helium-isotopes as tracers of trapped hydrothermal fluids in ocean-floor sulfides. Geology 22, 823–826.
Sun, S.S., Mcdonough, W.F., 1989. Chemical and isotopic systematics of oceanic basalts: implication for mantle composition and processes. Geol. Soc. Special Pub. 42, 313–345.
Tang, Y., Bi, X., Fayek, M., Hu, R., Wu, L., Zou, Z., Feng, C., Wang, X., 2014. Microscale sulfur isotopic compositions of sulfide minerals from the Jinding Zn–Pb deposit, Yunnan Province, Southwest China. Gondwana Res. 26, 594–607.
Tang, Y., Bi, X., He, L., Wu, L., Feng, C., Zou, Z., Tao, Y., Hu, R., 2011. Geochemical characteristics of trace elements, fluid inclusions and carbon-oxygen isotopes of calcites in the Jinding Zn-Pb deposit, Lanping, China. Acta Petrol. Sinica 27, 2635–2645 (In Chinese with English abstract).
Tang, Y., Bi, X., Wu, L., Wang, L., Zou, Z., He, L., 2013a. Re-Os isotopic dating of pyrite from Jinding Zn-Pb ore deposit and its geological significance. Acta Mineral. Sinica 33, 287–294.
Tang, Y., Bi, X., Wu, L., Zou, Z., He, L., 2013b. Carbon, oxygen, strontium and lead isotopic geochemistry in the Jinding super-large Zn-Pb deposit, Yunnan Province. Geochemica 42, 467–480 (In Chinese with English abstract).
Tao, X.F., Zhu, L.D., Liu, D.Z., Wang, G.Z., Li, Y.G., 2002. The formation and evolution of the Lanping basin in western Yunnan. J. Chengdu Univ. Technol. 29, 521–525 (in Chinese with English abstract).
Tao, Y., Bi, X.W., Xin, Z.L., Zhu, F.L., Liao, M.Y., Li, Y.B., 2011. Geology, geochemistry and origin of Lanuoma Pb-Zn-Sb deposit in Changdu area, Tibet. Miner. Deposits 30, 599–615 (in Chinese with English abstract).
Taylor, H.P.J., 1974. The application of oxygen and hydrogen isotope studies to problems of hydrothermal alteration and ore deposition. Econ. Geol. 69, 843–883.
Teng, Y.G., Liu, J.D., Zhang, C.J., Ni, S.J., Peng, X.H., 2001. Trace element characteristics of magmatic rock series in Lanping Basin and its neighboring areas. J. Chengdu Univ. Technol. 28, 40–44 (in Chinese with English abstract).
The Yunnan Jinding Zn Ltd Corporation, 2008. Checked Report on the Resources of Beichang-Jiayashan Section, Jinding deposit (unpublished).
Third Geological Team, 1984. The exploration report of the Jinding Zn-Pb deposit in Lanping County, Yunnan Province. Yunnan Bureau of Geology and Mineral Resources Open-file Report.
Tian, S.H., Yang, Z.S., Hou, Z.Q., Liu, Y.C., Gao, Y.G., Wang, Z.L., Song, Y.C., Xue, W.W., Lu, H.F., Wang, F.C., Su, A.N., Li, Z.Z., Wang, Y.X., Zhang, Y.B., Zhu, T., Yu, C.J., Yu, Y.S., 2009. Rb-Sr and Sm-Nd isochron ages of Dongmozhazhua and Mohai laheng Pb-Zn ore deposits in Yushu area, southern Qinghai and their geological implications. Miner. Deposits 28, 747–758 (in Chinese with English abstract).
Turner, G., Stuart, F.M., 1992. Helium/heat ratios and deposition temperatures of sulphides from the ocean floor. Nature 357, 581–583.
Wang, G.H., 2010. A genetic study on the Jinman-Liancheng vein Cu deposits in the northwestern Yunnan (Master Thesis). Kunming University of Science and Technology, Kunming (50 pp.) (in Chinese with English abstract).
Wang, A.J., Cao, D.H., Gao, L., Wang, G., Guan, Y., Xiu, Q., Liu, J., 2009a. A probe into the genesis of jinding super-large lead-zinc ore deposit. Acta Geol. Sinica 83, 43–54.
Wang, J.B., Li, C.Y., 1991. REE geochemistry of the Jinding super-large Pb-Zn deposit. Geochimica 20, 359–365 (in Chinese with English abstract).
Wang, X., Hou, Z., Song, Y., Yang, T., Zhang, H., 2011. Baiyangping Pb-Zn-Ag-Cu polymetallic deposit in Lanping basin: metallogenic chronology and regional mineralization. Acta Petrol. Sinica 27, 2625–2634 (in Chinese with English abstract).
Wang, C.M., Sagas, L., Lu, Y.J., Santosh, M., Du, B., McCuaig, T.C., 2016. Terrane boundary and spatio-temporal distribution of ore deposits in the Sanjiang Tethyan Orogen: insights from zircon Hf-isotopic mapping. Earth-Sci. Rev. 156, 39–65.
Wang, X.L., Yang, S.S., Pang, Y.C., Fu, X.G., Li, D.L., 2009b. Ore sources and organic mineralization in the Jinding lead-zinc deposit, Yunnan Province. J. Earth Sci. Environ. 31, 376–382 (in Chinese with English abstract).
Wang, Y., Zeng, P., Li, Y., Tian, S., 2004. He-Ar isotope composition of Jinding and Baiyangping mineral deposit and its significance. J. Mineral. Petrol. 24, 76–80 (in Chinese with English abstract).
Wen, C.Q., Cai, J.M., Liu, W.Z., Qin, G.J., Cheng, S.F., 1995. Geochemical characteristics of fluid inclusions in the Jinding lead-zinc deposit, Yunnan, China. J. Mineral. Petrol. 15, 78–84 (in Chinese with English abstract).
Wilkinson, J.J., 2010. A review of fluid inclusion constraints on mineralization in the Irish ore field and implications for the genesis of sediment-hosted Zn-Pb deposits. Econ. Geol. 105, 417–442.
Wu, G.G., Wu, X.D., 1989. A preliminary study on the tectonic evolution and mineralization regularity of the Jinding lead-zinc deposit, Yunnan province. Earth Sci. 14, 477–486 (in Chinese with English abstract).
Xiu, Q.Y., Wang, A.J., Gao, L., Liu, J.L., Yu, C.L., Cao, D.H., Fan, S.J., Zhai, Y.F., 2006. Discussion on the geologic time of host rocks of Jinding super large deposit and its geological implications. Geol. Surv. Res. 29, 294–302 (in Chinese with English abstract).
Xue, C.J., Chen, Y.C., Wang, D.H., Yang, J.M., Yang, W.G., 2003. Geology and isotopic composition of helium, neon, xenon and metallogenic age of the Jinding and Baiyangping ore deposits, northwest Yunnan, China. Sci. China (Series D) 46, 789–800.
Xue, C.J., Chen, Y.C., Yang, J.M., Wang, D.H., 2002. Jinding Pb-Zn deposit: geology and geochemistry. Miner. Deposits 21, 270–277 (in Chinese with English abstract).
Xue, C.J., Zeng, R., Liu, S.W., Chi, G.X., Qing, H.R., Chen, Y.C., Yang, J.M., Wang, D.H., 2007. Geologic, fluid inclusion and isotopic characteristics of the Jinding Zn-Pb deposit, western Yunnan, South China: a review. Ore Geol. Rev. 31, 337–359.
Yang, Y.B., 2013. Studies on chacterization, source and evolution of the Mesozoic-Cenozoic ore-forming fluids in the Lanping Basin (Master Thesis). Kunming University of Science and Technology, Kunming, pp. 90 (in Chinese with English abstract).
Ye, Q.T., Hu, Y.Z., Yang, Y.Q., 1992. Regional Geochemistry Background and the Gold-silver-lead-zinc Mineralization in Sanjiang Area. Geological Publishing Press, Beijing, pp. 217–264 (in Chinese).
Yin, H.H., Fan, W.M., Lin, G., 1990. The deep factor of geodepression basin evolution and the mineralization of crust-mantle mixing in Lanping-Simao, Yunnan. Tectonics Metallogenic Geol. 14, 113–124 (in Chinese with English abstract).

Zeng, R., 2007. The large scale fluid ore-forming process in the Lanping basin-taking the Jinding and Baiyangping deposits as the examples (Ph.D Thesis). Chang'an University, Xi'an (82 pp.) (in Chinese with English abstract).
Zhang, C.J., Ni, S.J., Teng, Y.G., Peng, X.H., Liu, J.D., 2000. Relationship between Himalayan tecotonomagmatic movement and mineralization in Lanping basin, Yunnan Province. J. Mineral. Petrol. 20, 35–39 (in Chinese with English abstract).
Zhang, F., Tang, J.X., Chen, H.D., Fan, X.H., Chen, S.H., Chen, W.B., Wang, C.H., Xie, H., 2010. The evolution and the metallogenic characteristic of Lanping basin. Geol. Explor. 46, 85–92 (in Chinese with English abstract).
Zhang, J., Wen, H., Qiu, Y., Zhang, Y., Li, C., 2013. Ages of sediment-hosted Himalayan Pb–Zn–Cu–Ag polymetallic deposits in the Lanping basin, China: Re–Os geochronology of molybdenite and Sm–Nd dating of calcite. J. Asian Earth Sci. 73, 284–295.
Zhang, J.R., Wen, H.J., Qiu, Y.Z., Zou, Z.C., Du, S.J., Wu, S.Y., 2015. Spatial–temporal evolution of ore-forming fluids and related mineralization in the western Lanping basin, Yunnan Province, China. Ore Geol. Rev. 67, 90–108.
Zhang, Q., 1993. Pb isotopic composition of Jinding super-large Pb-Zn deposit in Yunnan Province and discussion on the source of lead. Geol. Prospect. 29, 21–28 (in Chinese with English abstract).
Zhang, Q., Liu, J.J., Shao, S.X., Liu, Z.H., 2002. An estimate of the lead isotopic compositions of upper mantle and upper crust and implications for the source of lead in the Jinding Pb-Zn deposit in Western Yunnan, China. Geochem. J. 36, 271–287 (in Chinese with English abstract).
Zhao, H., 2006. Study on the characteristics and metallogenic conditions of copper-polymetallic deposits in middle-northern Lanping basin, western Yunnan (Ph.D Thesis). China University of Geosciences, Beijing (109 pp.) (in Chinese with English abstract).
Zhao, X., 1989. Stable isotope geochemistry of the Jinding lead-zinc ore deposit, Yunnan. Earth Sci. 14, 495–502 (in Chinese with English abstract).
Zhao, X., 1990. The Jinding lead-source of lead-zinc deposit, Lanping County. Yunnan Geol. 9, 26–36 (in Chinese with English abstract).
Zou, Z.C., 2013. The ore-forming fluid and metallogenic mechanism of the Ag–Cu polymetallic ore deposits at the Baiyangping area, the Lanping basin, Yunnan Province, China (Ph.D thesis). The University of Chinese Academy of Sciences, Beijing, p. 128 (in Chinese with English abstract).
Zhou, W.Q., Zhou, Q.L., 1992. A study on the isotope composition of Pb and S in the Lanping Pb-Zn deposit, Yunnan Province. Geochemica 2, 141–148 (in Chinese with English abstract).
Zou, Z., Hu, R., Bi, X., Wu, L., Feng, C., Tang, Y., 2015. Absolute and relative dating of Cu and Pb-Zn mineralization in the Baiyangping area, Yunnan Province, SW China: Sm-Nd geochronology of calcite. Geochem. J. 49, 103–112.